Near-Highway Aerosol and Gas-phase Measurements in a High Diesel Environment

DeWitt H.L.[1], Hellebust S.[1], Temime-Roussel B.[1], Ravier S.[1], Polo L.[2,3], Jacob V. [2], Buisson C.,

Charron A.[3], André M. [3], Pasquier A.[3], Besombes J.L.[4], Jaffrezo J.L.[2], Wortham H.[1], Marchand N.[1]

[1]Aix Marseille Université, CNRS, LCE FRE 3416, 13331 Marseille, France
[2] Université Grenoble Alpes, CNRS, LGGE, F-38000 Grenoble, France
[3] IFSTTAR, Case 24, 69675 Bron Cédex, France
[4] Université de Savoie, LCME, 73376 Le Bourget du lac, France

Corresponding authors: H. Langley DeWitt (Helen-Langley.Dewitt@univ-amu.fr) and Nicolas Marchand (Nicolas.Marchand@univ-amu.fr).

Abstract

Diesel-powered passenger cars currently outnumber gasoline-powered cars in many countries, particularly in Europe. In France, diesel cars represented 61% of light duty vehicles in 2011 and this percentage is still increasing (French Environment and Energy Management Agency, ADEME). As part of the September 2011 joint PM-DRIVE (Particulate Matter- DiRect and Indirect on-road Vehicular Emissions) and MOCOPO (Measuring and mOdeling traffic COngestion and POllution) field campaign, the concentration and high-resolution chemical composition of aerosols and volatile organic carbon (VOC) species were measured adjacent to a major urban highway south of Grenoble, France. Alongside these atmospheric measurements, detailed traffic data were collected from nearby traffic cameras and loop detectors, which allowed the vehicle type, traffic concentration, and traffic speed to be quantified. Six aerosol age and source profiles were resolved using the positive matrix factorization (PMF) model on real-time high-resolution aerosol mass spectra. These six aerosol source/age categories included a hydrocarbon-like organic aerosol (HOA) commonly associated with primary vehicular emissions, a nitrogen containing aerosol (NOA) with a diurnal pattern similar to that of HOA, oxidized organic aerosol (OOA), and biomass burning aerosol (BBOA). While quantitatively separating influence of diesel versus gasoline proved impossible, a low HOA: Black Carbon ratio, similar to that measured in other high-diesel environments, and high levels of NOx, also indicative of diesel emissions, were observed. Although the measurement site was located next to a large source of primary emissions, which are typically found to have low oxygen incorporation, OOA was found to comprise the majority of the measured organic aerosol, and isotopic analysis showed that the measured OOA contained mainly modern carbon, not fossil-derived carbon. Thus, even in this heavily vehicular-emission impacted environment, photochemical processes, biogenic emissions, and aerosol oxidation

55 dominated the overall organic aerosol mass measured during most of the campaign.

56 **1. Introduction**

57 Aerosols are known to have adverse effects on human health and on the global climate. The
58 World Health Organization (WHO) recently added anthropogenic aerosol and air pollution to their list
59 of known carcinogens (WHO, 2013), and high mass concentrations of particles less than 2.5
60 micrometers in diameter (PM2.5), such as those emitted by vehicular combustion processes, are
61 particularly harmful (Lighty et al., 2000)**.** Vehicular traffic is a large source of submicrometer
62 anthropogenic aerosol and proximity to large sources of vehicular emissions has been shown to
63 increase lung and heart disease, especially in children (Brugge et al., 2007). A recent WHO report
64 examined the toxilogical effects of black carbon (BC) aerosol, a known emission of diesel vehicles.
65 Although no difference in toxicology between PM2.5 and BC aerosol inhalation was found, BC was
66 cited as a marker for more general vehicular emissions, which have been shown to have negative health
67 effects; diesel exhaust was added as a known carcinogen the year before general air pollution and
68 PM2.5 (Janssen, World Health Organization, 2012). Aside from the potential detrimental health
69 effects of BC, BC also has significant implications for climate change. Unlike the majority of aerosol
70 (e.g., most organic aerosol, ammonium sulfate, ammonium nitrate), BC aerosol is associated with
71 global warming due to its high absorption of solar radiation (Bond et al., 2013). Diesel vehicles have
72 been singled out as important sources of BC to regulate as, unlike most other BC sources, diesel
73 vehicles tend not to co-elute high concentrations of other, less absorbing (thus more cooling) aerosol
74 and therefore have a higher net heating effect than mixed-emission black carbon sources (Bond et al.,
75 2013).

76 In France, the lower cost of diesel fuel (due to a lower taxation rate of diesel fuel versus
77 gasoline fuel) and the generally higher fuel efficiency of diesel engines have increased the popularity of
78 diesel passenger cars. In 2011, 82% of the fuel consumed in France was diesel (World Bank, 2011).
79 For comparison, this percentage in 2011 was 28% in the US, 57% in China, 70% in the European

Union, 49% in Latin America and the Middle East, and 83% in low-income countries.

The emission characteristics and emission limits of these two types of engines (diesel and gasoline) are quite different: diesel vehicles have higher emission factors for primary organic aerosol (POA) and BC, while gasoline-powered vehicles have higher emission factors for carbon monoxide (CO), carbon dioxide (CO_2), and volatile organic carbon (VOCs) (e.g., trimethylbenzene, benzene) (Platt et al., 2013). Black carbon, in particular, is closely associated with diesel: in Europe, North America, and Latin America, an estimated 70% of BC emissions are from diesel-powered vehicles (Bond et al., 2013). In Marseille, France, a traffic tunnel experiment measured an organic carbon/elemental carbon ratio (OC/EC) in PM2.5 of 0.3-0.4, which indicates that significant amounts of black carbon is emitted from local traffic in Marseille (El Haddad et al., 2009). Recent measures have been taken in Europe to reduce the particulate emission from diesel vehicles: from Euro 4 to Euro 5, a diesel particle filter (DPF) was introduced in diesel vehicles and the regulated emission limit for PM2.5 was halved for diesel cars and trucks.

Aerosol and VOC emissions from both vehicle types, as well as biogenic emissions, industrial emissions, and emissions from other sources, will react together in the atmosphere and potentially form secondary organic aerosol (SOA). Thus, primary aerosol emissions may not be the most important emission factor to take into account for global reduction in anthropogenic aerosol. After emission, VOCs can react in the atmosphere and form SOA. From these reactions, gasoline VOC emissions could ultimately lead to the formation of higher concentrations of organic aerosol than organic aerosol released directly from diesel vehicles, as reported in a recent study comparing the SOA formation from a Euro 3 diesel LDV and a Euro 5 gasoline LDV (Platt et al., 2013).

A recent study by Bahreini et al. (2012) measured similar levels of SOA in the heavily traffic-influenced LA Basin during both weekend and weekday afternoons. While diesel-powered vehicle numbers on the road decrease significantly on the weekends in the LA area, the measured SOA does not, which leads to the conclusion that gasoline emissions are more responsible for SOA than diesel

105 emissions (Bahreini et al., 2012). Nordin et al. (2013) performed smog-chamber studies on SOA
106 formation from gasoline-vehicle VOC emissions during simulated cold start and idling driving
107 conditions, and confirmed the high potential of SOA formation from gasoline car exhaust. Another
108 recent paper calculates the reactivity potential of diesel and gasoline fuel and comes to the opposite
109 conclusion: that due to the reactivity potential of diesel fuel, diesel-powered vehicles should contribute
110 greater amounts of SOA than gasoline-powered vehicles to the atmosphere (Gentner et al., 2012). Thus,
111 controversy still exists regarding the eventual aerosol emission factors of diesel and gasoline engines
112 when considering both primary emissions and potential SOA formation.

113 Finally, gas-phase NO and NO_2 (NOx) ambient concentrations are also mostly associated with
114 diesel fuel use (Vestreng et al., 2009). Throughout Europe, while NOx emission standards for diesel
115 vehicles have increased in stringency in recent years, ambient NO_2 levels have not shown a
116 corresponding decrease (Vestreng et al., 2009). The reduction of atmospheric NOx is important for
117 health-related reasons as an increase in NOx leads to an increase in tropospheric ozone, which is a
118 known lung irritant. NOx levels have also been shown to affect the formation rate, formation pathways,
119 and chemical composition of secondary organic aerosol from the reaction of primary species in
120 numerous chamber studies (Carlton et al., 2009; Kroll et al., 2005; Ng et al., 2007, 2008; Presto et al.,
121 2010).

122 European vehicular emissions, near-highway pollution levels, and the chemical composition of
123 highway pollution may be quite different than those measured in North America due to many factors,
124 including: 1) different emission standards and fuel regulations in the two regions 2) different after-
125 treatment devices to reduce the emission of certain pollutants and 3) a much larger percentage of
126 diesel-powered passenger cars on the road. A comparison between European and North American
127 near-highway measurements could lead to further understanding of the effects of diesel versus gasoline
128 on near-highway atmospheric chemistry.

129 To fully categorize the aerosol, VOC, and NOx emissions of traffic in France, the joint PM-

DRIVE (Particulate Matter- DiRect and Indirect on-road Vehicular Emissions) and MOCOPO (Measuring and mOdeling traffic COngestion and POllution) field mission took place in the Grenoble basin, France during the fall of 2011 at a near-highway location south of the city center. During the field measurements discussed in this paper, traffic cameras allowed vehicle type determination through license plate automatic identification. Traffic densities, speed and total flow were quantified through loop detectors, while measurements of the chemical composition, concentration, and size of aerosol were collected using both real-time and offline analysis, and parallel data on the gas-phase chemical composition of the roadway-adjacent environment were also collected. A source apportionment model was applied to real-time aerosol chemical composition data. Particular attention was paid to the chemical composition of particles and VOCs emitted during morning and evening rush hours in an attempt to elucidate the primary vehicular influence on near-highway air pollution.

2. Experimental Methods

2.1. Description of the Measurement Site

The sampling site was located at 45.150641 N, 5.726028 E (Figure 1), just south of Grenoble, France adjacent to a major highway (south of E712, with A480 2 km to the east). During the week, the total traffic on the highway was about 95,000 vehicles day^{-1} (65,000 during the weekend). Grenoble, a large city with over half a million people, is located in the southeast of France at the foothills of the Alps. The surrounding mountain ranges both buffer the Grenoble area from the effects of transported aerosol and can also trap pollution within the valley, particularly during the winter months and periods of temperature inversions. The isolating effect of the mountains thus simplifies the potential sources for aerosol, making it an interesting location for the study of specific aerosol emission sources.

2.2. Traffic Cameras and Loop Detectors

Traffic cameras mounted to a roadway sign were used to capture the license plate numbers of vehicles driven on the highway close to the field measurement site. These numbers were later used to classify vehicular traffic into different categories: vehicle type (LDV, Heavy duty vehicles (HDV),

buses) and age, vehicle size and engine capacity, fuel type (diesel or gasoline), and Euro number (i.e. the pollutant emission regulation that the vehicle complies with), The speed of the passing vehicles was also monitored with the classical traffic detector (double electromagnetic loops, able to identify the passing of all vehicles and their speeds), which allowed the identification of periods of stop-and-go, dense, or free-flow traffic.

2.3. Massalya Platform

The MASSALYA platform is a mobile laboratory equipped for air quality measurements with a hub located at the Aix Marseille Université. For the field campaign, PM2.5 and PM1 sampling heads situated above the roof of the stationary truck were connected to a variety of online instrumentation located within the truck body. Complementary off-line analysis was performed on filter samples collected by HiVol samplers located adjacent to the MASSALYA platform. All sampling occurred approximately 15 m from one of the traffic lines, as shown in Figure 1. Further details can be found in Polo-Rehn, (2013).

A High-Resolution Time-of-Flight Aerosol Mass Spectrometer (Aerodyne, HR-ToF-AMS) was used to analyze the chemical composition, size, and concentration of non-refractory submicrometer particles in the ambient atmosphere (DeCarlo et al., 2006). Instrument specifications have been discussed in detail elsewhere (DeCarlo et al., 2006). Briefly, both high resolution and size-speciated chemical information for ambient aerosol were obtained from this instrument. Aerosols were vaporized at 600 ^{o}C, ionized using electron ionization (EI) at an energy of 70 eV, and the chemical composition of bulk aerosol was measured using a ToF mass spectrometer (TOFWERK). Aerosol spectra were continuously collected and a two-minute average spectrum was obtained. Aerosol vacuum aerodynamic diameter was calculated by setting a particle start time using a chopper wheel and measuring the particle flight time along the particle ToF (pToF) sizing region (DeCarlo et al., 2006). Typical resolution during the campaign was around 2800 m/Δm (where m=*m/z* and Δm=full-width at half max of the mass peak).

In addition to the HR-ToF-AMS, a Size-Mobility Particle Scanner (TSI, SMPS) was used to measure the size distribution and concentration of ambient aerosol and a Multiangle Absorption Photometer (Thermofischer, MAAP 5012) was used to measure the concentration of black carbon.

High resolution mass spectra of VOCs were obtained using an Ionicon Proton-Transfer Reaction Time of Flight Mass Spectrometer 8000 (PTR-ToF-MS, hereafter referred to as PTR-MS) (Graus et al., 2010). The PTR-MS analyzes trace (parts per trillion by volume) VOCs with high mass resolution, which allows the separation of different species with the same nominal mass and the identification of each peak's elemental formula. The PTR-MS was run with a 25 second time resolution and a flow of 100 cm^3 min^{-1}. Drift tube parameters of the PTR-MS were as follows: Voltage: 560 V, Drift tube pressure: 2.11 mbar, Drift tube temperature: 333 K, resulting in an E/N (electric field/number concentration of neutral particles) of 133 Td.

The SMPS, PTR-ToF-MS, and HR-ToF-AMS were connected to the same sample inlet with a PM2.5 sampling head and a sample flow of 1 m^3 hr^{-1}. Particles were dried (RH<30%) using a Nafion dryer prior to measurement with the HR-ToF-AMS and SMPS. The MAAP was connected to a separate PM1 sampling head. PM1 filter HiVol (30 m^3 h^{-1}) samples were collected on quartz filters (Tissuquartz) on a daily basis and analyzed for radiocarbon isotope data. Radiocarbon measurements were conducted using ARTEMIS Accelerator Mass Spectrometry, at Saclay (CNRS-CEA-IRD-IRSN, France) on the total carbon (TC) fraction after a combustion of the samples at 850°C. The method is fully described in El Haddad et al. (2011).

A Young meteorological station was also installed to capture wind speed, wind direction, relative humidity, and temperature data at the measurement location.

2.4. Air Rhône Alpes station

Twenty meters east of the Massalya platform, still adjacent to the highway, the Air Rhône Alps station collected PM2.5 HiVol (30 m^3 h^{-1}) samples on quartz fiber filters (Tissuquartz) with a time

205 resolution of 4 hours. PM2.5 samples were analyzed for EC/OC, inorganic ions, and targeted organic
206 tracers (Polo-Rehn, 2013).
207 Organic compounds in these PM samples were also quantified by gas chromatography coupled
208 with mass spectrometry (GC-MS), following the method detailed in El Haddad et al. (2009) and Favez
209 et al. (2010). EC and OC measurements were performed using the Thermo-Optical Transmission (TOT)
210 method on a Sunset Lab analyzer (Birch and Cary, 1996; Jaffrezo et al., 2005) following the
211 EUSAAR2 temperature program (Cavalli et al., 2010). Ionic species were analyzed with Ionic
212 Chromatography (IC) following the method described in Jaffrezo et al. (1998).
213 All filters used in this study were preheated at 500 ^{o}C during 3 h. Samples were stored at -18 ^{o}C
214 in aluminum foil and sealed in polyethylene bags until analysis.
215 In addition, NOx (NO and NO_2), PM10 and PM2.5 mass concentrations were measured and a
216 Tapered Element Oscillating Microbalance equipped with a Filter Dynamic Measurement System
217 (TEOM-FDMS, Thermo Scientific) for real-time measurements of PM10 and PM2.5.
218 **3. Results and Discussion**
219 *3.1 Traffic Conditions at the Measurement Site*

220 A detailed view of the measured traffic is presented in the supplementary information (Figure
221 S1). Briefly, the overall makeup of the traffic remained fairly steady throughout the campaign. The
222 bulk of the vehicles directly affecting the measurement site were Euro 4 (released in 2005) or older;
223 thus, the most recent emission regulations had only a small effect on the air quality around the field site.
224 The ratio between diesel and gasoline cars was found to be 2.6, or 72% diesel, with a high correlation
225 (R^2=0.96) between diesel and gasoline vehicles.
226 *3.2. General atmospheric conditions and aerosol and VOC concentrations and evolution*
227 Wind speeds were generally low throughout the campaign (<1-2 m/s) with higher wind speeds
228 peaking in the afternoons and tapering off in the evenings. The wind direction was primarily from the

229 northwest, from the direction of the nearby highway. A diagram of the two measurement stations, the
230 wind rose plot for the Massalya location, and polar plots showing the concentration of NO and BC as a
231 function of wind direction are shown in Figure 1. BC and NO were associated with all wind directions,
232 though slightly higher from the highway direction, which suggested that the measurement site was
233 directly and strongly influenced by the traffic emissions. However, in order to better describe the traffic
234 influence, we defined high traffic periods (HT) within the dataset. These HT periods were selected as
235 follows : wind direction >40 or <320, NO in the 75th percentile, and from 6:30-9:30 or 17:00-20:00
236 (rush hour periods). The fixed location of the measurement stations made determination of
237 concentration drop-off as a function of distance from the roadway impossible to determine with the
238 dataset, although that has been shown to be important in other studies (such as Karner et al., 2010).
239 However, the measurements were all taken closer to the roadway (~15 m) than the calculated distance
240 where roadway emission drop off to background levels (115-570 m, Karner et al., 2010).
241 The campaign time series concentration of submicrometer non-refractory aerosol sulfate (SO_4),
242 ammonium (NH_4), nitrate (NO_3), and organic species from the HR-ToF-AMS is shown in Figure 2A.
243 The limit of detection for each species was calculated using the method described byDeCarlo et al.
244 (2006) and found to be 0.30, 0.21, 0.06, and 0.33 μg m^{-3} for SO_4, NH_4, NO_3, and organic aerosol,
245 respectively, for our measurements with a time resolution of 2.5 min. A collection efficiency (CE) of
246 0.75 was applied to HR-ToF-AMS aerosol concentration measurements taken during this campaign.
247 The CE factor compensates for incomplete vaporization of non-refractory species due to particle
248 bounce, the likelihood of which changes with particle phase and chemical speciation (Huffman et al.,
249 2005; Matthew et al., 2008). This CE was calculated by comparing the HR-ToF-AMS SO_4
250 concentrations to 4 hour filter concentrations (Figure S2). This comparison gave a value of 0.75±0.03
251 for the slope between the two types of measurements.
252 PM2.5 averaged 17 μg m^{-3} for the campaign (Figure S3) while PM10 averaged 22 μg m^{-3}.

These values increased slightly during HT periods (a 1.3 and 1.25x increase, respectively). Black carbon and organic aerosol species dominated the measured aerosol composition throughout the campaign, and comprised 39 and 40% of the total speciated submicrometer aerosol, respectively. PM2.5 had a somewhat higher mass variation than the AMS + BC measured mass (Figure S3), likely due to the smaller measurement size cutoff for AMS (1 μm) and the presence of road dust in the local environment, a large portion of which may be non-refractory and those unable to be measured by the AMS. Increases in BC and the aerosol marker *m/z* 57 ($C_4H_9^+$), a marker for primary organic carbon in the HR-ToF-AMS (Zhang et al., 2005), correlated in time to the observed morning and evening traffic peaks (Figure 2B), with BC levels reaching 10-16 μg m^{-3} during the mornings (Figure 2A) for 2.5 min averaged measurements. As expected, an increase of BC and m/z 57 (1.5x) was observed during HT periods. Note that BC concentrations during high filter loadings (BC accumulation rate > 0.14 μg min^{-1}) have been removed to compensate for the underestimation of BC by the MAAP during periods of high concentrations (Hyvärinen et al., 2013). Along with increased concentrations of *m/z* 57 and BC, elevated number concentrations of small particles (up to 1-2x10^5 cm^{-3} during peaks from daily base levels of 2-4x10^4 cm^{-3}) were observed during periods of HT (Figure 2D), for 5 min measurements. BC and *m/z* 57 had similar daily averages throughout the campaign; however, overall organic concentration rose significantly during the period from 9/12-9/14, when particle growth events were observed (Figure 2D). The geometric number mode diameter rose over the course of each day to a maximum diameter each afternoon, when photochemical processing was the most intense. A marker for oxidized, aged organic aerosol (Figure 2C, *m/z* 44, COO^+) also rose in concentration during this time period, further confirming that the larger aerosol and higher organic mass concentrations were due to aging and secondary organic aerosol formation processes. A period of heavy rain on the 18th and 19th of September removed much of the organic aerosol from the local atmosphere. Black carbon concentrations and small particle concentrations quickly returned to their previous levels. A new

277 accumulation period was observed after rainfall (Figure 2D), with the mode diameter of particles
278 increasing as secondary aerosol was formed again. The slow rise of organic concentration during these
279 periods, the lower BC:Org ratio, the enhancement of organic concentration outside of normal traffic
280 periods, and the low level of NO during these accumulation periods all suggest that this increase in
281 organic aerosol concentration was driven by regional influences, not by nearby vehicular emissions and
282 a more southerly wind direction during this time confirmed the transport of non-highway air masses to
283 the measurement site.

284 These findings are similar to those presented recently by Sun et al., (2012), who measured
285 aerosol size and chemical composition adjacent to the Long Island Expressway in New York and
286 observed that traffic-influenced aerosol emissions were primarily small particles which varied in
287 concentration with changes in traffic throughout the day. During periods with less traffic influence,
288 more oxygenated organic aerosol (OOA) and inorganic ions with larger mode diameters and lower
289 temporal variations were observed (Sun et al., 2012).

290 The time series concentrations of selected VOC peaks are shown in Figure 3. Primary traffic
291 related VOC species, such as aromatics (benzene and trimethylbenzene), were found to have high
292 temporal variations similar to those of traffic-related aerosol species and NOx (Figure 4C and D). NOx
293 levels were often over 400 ppbv during the morning rush hours, while the PTRMS peak corresponding
294 (in part) to toluene and benzene peaked around 2 to 1 ppbv (respectively). During a recent chamber
295 study in Ispra, Italy, fresh diesel emissions PTR-MS VOC spectra were found to contain peaks with the
296 same mass as $CH_4NO_2^+$ and $C_2H_5O^+$ (Hellebust et al., 2013, 2015), not present in fresh gasoline
297 emissions. These same peaks were also observed during this work and found to vary with traffic
298 during this measurement period, but had a smoother variation than the observed aromatics (Figure 3B).
299 While this species is unique for fresh diesel emissions versus gasoline emissions, aging processes occur
300 rapidly and other sources may contribute to this mass peak. Thus, these species, while increasing with
301 traffic, cannot be assumed to be tracers for primary diesel emissions in particular; no high-

concentration unique tracer peak for diesel VOC emissions was resolved from the fresh diesel emission spectra in these chamber experiments (Hellebust et al., 2015). A slight increase of the traffic related VOCs (1.2x for benzene and trimethylbenzene) was observed during HT periods compared to the campaign average. For $CH_4NO_2^+$ this relative increase during HT periods is lower (8%), which could confirm multiple sources of this compound.

In addition to traffic-related VOC emissions, mass peaks corresponding in exact mass to biogenic emissions, such as isoprene, were measured in ppbv levels. These peaks were found to rise in concentration with the ambient temperature (Figure 3A), typical of isoprene peaks. The presence of isoprene and its oxidation product, methyl vinyl ketone (MVK) or its isomer methacrolein (MACR), in similar concentrations as that of the major traffic-related VOC peaks (ppbv levels) suggested that biogenic emissions also significantly influenced the local atmosphere despite close proximity to anthropogenic emission sources (i.e., road traffic).

The high morning concentrations of traffic-related pollutants, compared to evening concentrations, were caused in part by a low early morning boundary layer that rose during the day and fell during the night. Boundary layer heights (BLH) were estimated using the Hybrid Single Particle Lagrangian Integrated Trajectory (HYSPLIT) backtrajectory model. The HYSPLIT model either extracts the BLH from meteorological file input into the model or, if no BLH exists in the meteorological file, BLH is estimated using the vertical temperature profile. A selection of the BLH-scaled diurnal profiles of traffic and biogenic emission related VOC concentrations are shown in Figure 4A along with traffic (speed, vehicular flux) diurnal profiles and the calculated boundary layer heights and measured temperatures (Figure 4B and C). This calculation was performed to more directly compare vehicle concentration and speed to vehicular emissions and temperature with biogenic emissions (by removing the dilution of emissions by the changing boundary layer height). Biogenic species, such as isoprene, peaked in concentration during the afternoon, when temperatures were the warmest. Aromatic species peaked in concentration, even after the rough boundary layer correction

was applied, during periods of low speeds. This is consistent with other findings that show cold starts and idling speeds cause an increase in aromatic VOC emissions from gasoline-powered vehicles (e.g., Broderick and Marnane, 2002).

3.3 PMF Analysis

The positive matrix factorization (PMF) model was applied to the HR-ToF-AMS aerosol data using the process described in detail by Ulbrich et al. (2009). Six aerosol factors were resolved by their source and relative aging using the PMF model: a hydrocarbon-like organic aerosol (HOA) factor, a regional oxidized organic aerosol (OOA) factor associated with sulfate aerosol, two oxidized organic aerosol factors with opposing diurnal patterns, one more oxidized than the other (Less Oxidized Organic Aerosol, or LO-OA, with peak concentration during the mornings/nights, and More Oxidized Organic Aerosol, or MO-OA, with peak concentrations during the afternoons), a biomass-burning organic aerosol factor (BBOA), and a nitrogen-containing organic aerosol factor (NOA). The mass spectra for the six resolved factors is shown in Figure 5, labeled with their identifications. Evaluation graphs for the six-factor PMF solution are shown in the Supplementary Information (Figures S5-S8). Polar plots of the factor concentrations and wind direction are shown in Figure S9. A six factor solution was the lowest number of factors where a BBOA factor was resolved; BBOA was suspected to be present in the air mass measured during the campaign due to periods of increased levoglucosan measured on filter samples. However, its concentrations were very low (15 ng m^{-3} on average, Polo-Rehn, (2013)) compared to concentrations measured in Grenoble in winter (around 800 ng.m^{-3} (Herich et al., 2014)). Solutions with more than six factors appeared to split the OOA factor further until differences between each OOA factor were difficult to justify. The calculated elemental ratios of O:C, H:C, and Organic Mass: Organic Carbon (OM:OC), (Aiken et al., 2008) are shown in Table 1.

The diurnal pattern and the relative concentrations of each resolved factor, averaged over the campaign period, are shown in Figure 6, along with the standard deviation of their concentrations.

Morning and evening peaks, correlating in time to rush hour traffic, were clearly observable for the HOA factor. Also clearly visible in Figure 6A is the opposing diurnal trends of LO-OA (peaking at night and early morning) and MO-OA (peaking around 3pm each afternoon). Regional OOA had no discernable diurnal trend. An interesting finding in these data is that the HOA and NOA factor concentrations both peaked during morning and evening high traffic periods (Figure 6A). This is not the general behavior demonstrated in most studies for the NOA factor, although a similar NOA factor has been previously measured in the Po Valley, Italy (Saarikoski et al., 2012). This behavior was confirmed by examining HT periods, with an increase of 1.3x and 1.9x for NOA and HOA concentrations, respectively, during HT periods. While many of the defined N-containing peaks were adjacent to or in between those of larger hydrocarbons or of other organics, only N-containing peaks whose fitting significantly reduced the residual mass at each unit mass were fit (Figure S8). Additionally, and when possible, the w-ToF mode data was examined to determine if the N-containing peak was resolved enough from neighboring peaks for certain identification.

In Figure 7, the time series of each factor are shown with oxalate ($C_2O_4^{2-}$, a marker for aged and oxidized organic aerosol), sulfates, and levoglucosan (a marker for biomass burning) measurements from filter samples. Table 2 summarizes the R^2 values between key tracer species and the resolved aerosol factors. The two main factors resolved, in terms of mass concentration, were the OOA factors with opposite diurnal trends, MO-OA and LO-OA. The concentration of MO-OA rose as the aerosol number-weighted geometric mode diameter rose, also indicative of increasing aerosol age/coagulation. The LO-OA factor resembled the SV-OOA factor reported by Docherty et al. (2008) measured during the Study of Organic Aerosols (SOAR) project at Riverside, CA, which was also found to decrease during the afternoon as temperature and photochemical processing increased. The chemical differences between these two spectra are show in Figure S10 and described in the Supplementary Information. The increase in MO-OA concentration occurred as both PTR-ToF-MS isoprene signal was increasing (also a temperature-related process) and as the 9-carbon aromatic: benzene ($C_9H_{13}^+$:$C_6H_7^+$) VOC ratio

was at its minimum (related to photochemical age of air mass, (Parrish et al., 2007) . Thus, the increase MO-OA could be linked to photochemical aging of vehicular emissions during the day and/or to increasing biogenic VOC emissions and their subsequent photochemical aging and condensation into aerosol form.

The BBOA factor was found to correlate with levoglucosan (R^2=0.65, n=38); while significant levels of biomass burning from wood-burning stoves and other combustion-related heating are known to affect the Grenoble Valley in winter, such a large contribution during this season is surprising. Likely the PMF-resolved BBOA factor was somewhat mixed with emissions with close spectral signature (vehicular emissions or potentially cooking aerosol emissions). Episodic local yard-waste burning could also have contributed to the bulk aerosol spectrum, as spikes in the BBOA concentration do not appear to correlate with a particular wind direction (Figure S9). The ratio of levoglucosan: BBOA is quite low (0.03); however, it is within the order of magnitude of previously reported measurements (e.g., 0.06, (Aiken et al., 2009)). Additionally, the higher levels of oxidants found in the atmosphere in the summer could cause a faster degradation of levoglucosan in the atmosphere after emission (Hennigan et al., 2010). Thus, the BBOA concentrations reported here shall be considered as an upper limit of the biomass burning contribution.

Of the factors resolved, the HOA factor had the lowest O: C ratio (0.07) and a good (R^2=0.58, n=3928) correlation with BC concentration. The mass spectrum of the resolved HOA factor highly resembled (R^2>0.95, n=100) previously resolved HOA factors and direct AMS measurements of diesel and gasoline emissions (Mohr et al., 2009; Zhang et al., 2005). HOA was not the largest average contributor to the bulk measured aerosol mass over the campaign period, despite the fact that these measurements were conducted 15 m from a major highway. The relative size of each type of particle (primary, or HOA, and OOA) likely played a major role in the relative mass concentrations of each factor (Figure S11 and discussion), and the higher increase above background of particle number versus particle mass found in this study agrees with previous studies (Karner et al., 2010, Sun et al.,

2010). The variability of each factor over the campaign was high as, unlike measurements in more rural areas, the proximity to a primary aerosol source (highway) and to an urban center (Grenoble), as well as large green spaces (the Alps) allowed the full range of aged and locally transported aerosol to be observed at this station.

3.3.1 Fossil and Modern Carbon

A source of uncertainty in the global particulate emissions of vehicles is the formation of SOA from gas-phase emissions and the aging of POA. To discriminate between the relative concentration of modern and fossil carbon, and thus potentially discriminate between OOA from vehicular sources and from modern sources, daily filter samples were collected at the sampling site and 14C radiocarbon measurements were performed. From these measurements, the percentage of modern carbon from TC (OC+EC) was calculated. Modern carbon varied from 15-36% of the total aerosol carbon, a significant portion of the measured carbon considering the close proximity of the measurements to fossil carbon sources. In France, the contribution of biofuel was about 7% and 5% for diesel and gasoline fuel, respectively, in 2011 (UFIP, Union Française des Industries Petrolières, 2011) and cannot explain this relative high proportion of modern carbon observed in the particulate matter. This is similar to findings shown in Hodzic et al. (2010), Minguillon et al. (2011), and El Haddad et al. (2013), which indicate that modern carbon is often more significant than fossil carbon in the carbonaceous fraction of PM, even in cities with high vehicular emissions (e.g., Mexico City, Barcelona or Marseille).

As radiocarbon measurements have been performed through a thermal approach (combustion of the samples at 850°C), we consider in the following section EC measured by the thermo-optical method. As shown in figure S12, EC and BC agree well at low mass loadings, but have a wider scatter in the data at higher mass loadings. The calculation of BC (measured by the MAAP) using an absorption cross-section is imprecise and, at high loadings of BC, may under or overestimate this mass loading. Figure S12 shows a comparison between the MAAP (BC) and thermal measurement (EC) data, with a 1:1 line. As the thermal-optical analysis of EC is a more direct analysis, EC was chosen to

427 be used in this calculation.

428

429 Assuming that the majority of EC was traffic-related, and thus from fossil origin, the
430 concentration of modern organic carbon and fossil organic carbon was then calculated. While evidence
431 for the presence of biomass burning aerosol was measured at the field site, the main source of EC was
432 likely diesel exhaust. Figure 8 shows the fraction of EC and OC, HOA, and a partitioning between
433 fossil and modern carbon. In Figure 8A, a rough calculation was performed to determine the
434 concentration of non-primary fossil organic carbon. For a first estimate, all EC was assumed to be
435 fossil in origin. Additionally, the HOA aerosol was also assumed to be vehicular, and thus fossil, in
436 origin. The HOA factor concentration has been divided by its OM: OC ratio to remove any non-carbon
437 mass (HOA C, calculated from the elemental formulas of the PMF factor mass spectra, Aiken et al.
438 (2008)). Both EC and HOA C had high (R^2=0.89 and 0.85 respectively, n=10) correlations with the
439 fossil C mass, which supported a largely fossil source for these two species. The remaining fossil
440 organic carbon mass after subtraction was then assumed to be from non-primary sources (in light blue).
441 This calculation provided a lower estimate of the amount of fossil carbon contributing to SOA
442 mass, and involves several assumptions and potential sources of error. Sources of error in this
443 calculation include error in the PMF resolution of primary (HOA) organic aerosol spectra and error in
444 the calculated OM:OC ratio of this factor species, biodiesel vehicular emissions contributing modern
445 carbon to measured HOA, and biomass burning aerosol contributing modern carbon to measured EC.
446 As the measured HOA:EC ratio was in-line with previous measurements in high diesel environments,
447 HOA concentrations did not appear to be significantly over or under estimated. Up to 7% of fuel use in
448 France was biodiesel, thus, part of the HOA concentration could be from modern sources. While
449 research has shown that the use of biodiesel fuels reduces the overall primary particulate matter
450 emissions (Cheung et al, 2010), biodiesel could still be a modern carbon contributor to OC and EC
451 mass. Additionally, although the concentration of BBOA was generally low (a campaign average of

452 0.34 ± 0.23 μg m^{-3}) and the ratio of BBOA:EC has been found to be on the order of 3-4 in other areas
453 of France (Crippa et al., 2013), some contribution to EC from biomass burning may have been present
454 at the measurement site. In Figure 8B, a range of fossil non-primary organic carbon, normalized to
455 total measured organic carbon, is presented. For the upper limit of this range, HOA C and EC were
456 considered to be 95% fossil and 5% modern (7% biodiesel fuel use and an estimated 25% reduction in
457 particulate emissions from biodiesel fuel). Also for this upper limit, the calculated concentration of
458 BBOA was divided by 3 and used to calculate possible modern EC from biomass burning (Crippa et al.,
459 2013).

460 Total organic carbon concentration appeared to be more driven by processed/aged OOA
461 concentrations than by primary emissions. During the period with the highest organic concentrations
462 (September 15^{th}-17^{th}), most of the non-HOA carbon measured was modern carbon. Also during this
463 time period, the winds were also slightly more southerly and SO_4 and OOA concentrations increased,
464 which could indicate a more regional contribution to the measured air mass during this time. After a
465 period of heavy rain on the 19^{th}, almost none of the non-HOA, organic carbon was fossil; however, this
466 also coincided with a period of increased BBOA, which may have contributed to modern-EC emissions
467 and thus an underestimate of fossil-OC emissions (Figure 7). At other times during the campaign,
468 HOA concentrations alone could not adequately explain all of the measured fossil organic carbon and
469 additional sources of fossil organic carbon (such as photochemical reactions forming aerosol from
470 vehicular VOC emissions) would be needed. Additionally, the origin of the NOA factor factor remains
471 unclear, and if fossil in origin, could explain part of the non-HOA organic fossil carbon measured at
472 the site, further reducing the OOA fossil-C (at times to almost zero). Overall, throughout the campaign
473 the majority of OOA observed was most probably modern in origin.

474 The high levels of modern carbon OOA suggested that biogenic compounds had a large effect
475 on the overall aerosol population in this location, even directly adjacent to a large anthropogenic
476 emission source (i.e., traffic). Interaction between anthropogenic oxidants and biogenic VOCs (or

477 BVOCs) has been found to increase the formation of SOA (Chameides et al., 1988; Goldstein et al.,
478 2009; Shilling et al., 2013), isoprene oxidation reactions leading towards SOA have been shown to vary
479 depending on the level of NOx (Chen et al., 2014; Kroll et al., 2005; Ng et al., 2007; Xu et al., 2014),
480 and likely BVOC concentrations were greater and the aromatic VOC concentrations were lower in the
481 wider Grenoble Valley.

482 *3.4.3. Differences between diesel-heavy and gasoline-heavy near-roadway measurements*

483 Older diesel vehicles have been shown to emit both higher levels of PM, particularly BC, and
484 higher levels of NOx. Indeed, high concentrations of NOx were measured at the field site, up to 450
485 ppbv ($NO+NO_2$) for 15 min averaged measurements. NO_2 levels exceeded the 100 ppbv European
486 hourly limit almost every morning. The campaign average for NO_2 was 94 +/- 64 ppbv. For
487 comparison, at a measurement site adjacent to a major highway in New York, Sun et al. (2012)
488 measured an average of 48 +/- 30 ppbv NO_2, about half that of this campaign's average, with 15 min
489 average peaks ranging from 100-300 ppbv. The hourly traffic concentrations at each site were close
490 (approximately 10,000 vehicles/hour reported during the Sun et al. (2012) measurement periods
491 compared to approximately 8,000 vehicles/hour observed during daylight driving hours on Grenoble's
492 highway); thus, increased NOx cannot be explained by increased traffic. Rather, increased diesel fuel
493 use is a very likely hypothesis.

494 High levels of BC were also measured in this work. A comparison of the HOA: BC ratio from
495 this study and from previously reported field studies is shown in Figure 9A. As expected, since the
496 French fleet includes a much higher percentage of diesel car with increased BC emissions, this ratio
497 was significantly lower than that reported for an urban-downwind site in Pittsburgh (1.41, Zhang et al.
498 (2005)), a highway adjacent site in New York (1.02, Sun et al. (2012)), an urban/highway site in
499 Ontario (0.7-1.1, Stroud et al. (2012)), a rural site in NW England (1.61-1.91, Liu et al. (2006)), and an
500 urban site in Zürich, Switzerland (1.1, Lanz et al. (2007)). As for measurements in France, a study in an
501 urban site in Paris observed a HOA:BC ratio of 0.61 (Crippa et al., 2013); this site was most probably

influenced by a vehicle fleet similar to Grenoble's, but measurements were collected during winter (lower temperatures) and within Paris (increased urban emissions). Tailpipe measurements of Euro 4 diesel and gasoline-powered vehicles (a Renault Kangoo and a Ford Ka, respectively) at IFSTTAR (Institut Français des Sciences et Technologies des Transports, de l'Aménagement et des Réseaux) performed during this PM Drive research program also show a much higher HOA: BC ratio for gasoline vehicles versus diesel vehicles (unpublished data). This was due to much higher BC emissions from the diesel vehicle, as opposed to higher HOA emissions from the gasoline vehicle. Similarly, the HOA factor measured near Grenoble was similar to that measured by Sun et al. (2012), in a high gasoline environment next to a highway in New York, both in absolute concentration and chemical composition; thus, an increase in BC emissions (from diesel) rather than a reduction in HOA: vehicle number was likely the cause of our low HOA: BC ratio.

The change in HOA: BC ratio as a function of the diesel: gasoline fuel use (Road sector, World Bank, 2011) is shown in Figure 9B. A decrease in HOA: BC with an increase in percent diesel is clearly observable with a strong correlation (R^2=0.85, n=10), despite the many different factors possibly influencing BC and HOA concentrations at each location (e.g., local aerosol sources, meteorology). Such a linear relationship between HOA: BC and diesel percentage is very interesting, but was not necessarily expected, since the emission factors of HOA+BC differ significantly between diesel and gasoline cars, especially for pre EURO5 vehicles.

Additionally, an AMS factor with a diurnal pattern peaking during rush hour and with N-containing peaks was observed. Saarikoski et al., (2012) found a similar amine-containing NOA factor in measurements taken in the Po Valley (Italy) that also had a strong diurnal pattern. However, their NOA factor was attributed to marine influence due to a correlation with MSA (Saarikoski et al., 2012), although it is possible that MSA was from the local industrial use of DMSO as a solvent, and had a higher H:C ratio (1.91) than the factor resolved from this data set (1.38). Like France, Italy has a large percentage of diesel fuel consumption (71%, World Bank 2011). Aiken et al., (2009) and Sun et al.,

(2011) also resolved N-containing OA factors from data measured in Mexico City and New York, respectively, but did not observe a similar diurnal pattern. In the PTR-ToF-MS mass spectra results obtained from Euro 5 vehicle emission smog chamber studies, Hellebust et al., (2015 and 2013) found higher nitrogen-containing emissions from fresh and aged diesel mass than from fresh and aged gasoline mass spectra (e.g., peaks such as $CH_4NO_2^+$). Similar nitrogen-containing VOC peaks were found by Inomata et al. (2013) in diesel exhaust. Thus, diesel-related emissions could possibly be the source for the observed NOA factor, although no significant correlation between this factor and other vehicular emissions, such as BC, was found. More detail on the NOA factor can be found in the Supplementary Information and Figure S13.

And finally, only small amounts OOA measured at the field site were calculated to contain fossil-OC. Work by Bahreini et al., (2010) found that much of the measured SOA in the Los Angeles Valley was from gasoline passenger cars, not from diesel trucks, and perhaps the relatively low concentration of gasoline vehicles on the road in France is related to the low concentration of fossil-OOA.

4. Conclusions

During this campaign, highly time resolved particle and gas-phase chemical composition and concentration measurements were obtained alongside parallel traffic data of the speed, fluxes, vehicle type, and fuel type of passing cars on a highway in the Grenoble Valley. An analysis of the local primary (traffic) aerosol and the more regional, aged secondary organic aerosol was performed for the PM1 fraction observed by the HR-ToF-AMS. The PMF model was run on the high-resolution HR-ToF-AMS aerosol data and six factors were resolved from the bulk aerosol data: 1) an HOA factor, related to traffic 2) a BBOA factor 3) a regional OOA factor, which covaried with sulfate 4) a MO-OA factor, increasing in concentration during sunny afternoons 5) a LO-OA factor, with the opposite diurnal pattern as MO-OA, likely due to gas-particle phase partitioning and photochemical processing

552 and 6) an NOA factor with a diurnal pattern similar to that of HOA and to traffic peaks.

553 The resolved mass spectrum for the HOA factor was chemically similar to mass spectra from
554 both gasoline and diesel-emitted organic carbon and previously resolved HOA factors in high-gasoline
555 environments; however, the HOA: BC ratio measured was low (<0.3) throughout the campaign. This
556 ratio agrees with previously reported HOA: BC ratios in high diesel environments and from direct
557 measurements of diesel emissions in smog chamber and tailpipe measurement studies. The fraction of
558 diesel-powered vehicles on the road appeared to control, to some extent, this ratio. Diesel also
559 influenced local NOx concentrations, as the measured NOx was two times higher than concentrations
560 near a similarly-trafficked highway in New York, USA.

561 While high levels of both black carbon (5 +/- 3 $\mu g\ m^{-3}$) and organic aerosol (8 +/- 4 $\mu g\ m^{-3}$)
562 were measured, when examined, only 20% of the total organic mass signal could be attributed to
563 primary vehicular emissions (i.e., HOA). Significant amounts of modern organic carbon were also
564 measured, and fossil carbon appeared to contribute only a small amount to the measured OOA.
565 Although NOx and VOCs emitted by diesel and gasoline engines, respectively, may have influenced
566 SOA formation in the Grenoble Valley, the majority of OOA measured was modern in origin, even
567 adjacent to a major source of fossil carbon. Whether this is due to a lower overall gas+particle
568 emission of diesel vehicles, the lack of aromatic compounds in diesel VOC emissions, high NOx
569 reducing the efficiency of vehicular VOC to SOA formation mechanisms, an acceleration of BVOC to
570 biogenic aerosol formation in the presence of vehicular emissions, or simply the more global source
571 and higher efficiency of BVOC to SOA reactions is unclear, but in a high diesel environment, SOA
572 OOA from fossil-fuel carbon was only a small source of the measured OOA , while modern C-
573 containing OOA dominated the organic aerosol mass in the fine fraction of PM1.

574

575

576

Acknowledgments:

This work was supported by the French Environment and Energy Management Agency (ADEME, Grant number 1162C0002). The authors gratefully acknowledge the NOAA Air Resources Laboratory (ARL) for the provision of the HYSPLIT transport and dispersion model (http://www.ready.noaa.gov) used in this publication. We also gratefully acknowledge Air Rhone Alpes staff (particularly Yann Pellan) for their support during the campaign as well as Y. Sun and Q. Zhang for providing near-highway aerosol data from their paper Sun et al., (2012) for comparison with these measurement, and the MASSALYA instrumental platform (Aix Marseille Université, lce.univ-amu.fr) for the analysis and measurements used in this publication. Finally, the authors would like to acknowledge and thank the two anonymous reviewers who provided constructive advice on the formation of the final paper.

595
596

597

598 Table 1

599

PMF FACTOR	OM:OC	H:C	O:C
HOA	1.25	1.89	0.07
NOA	1.69	1.38	0.4
LO-OA	1.74	1.34	0.47
MO-OA	2.15	1.16	0.78
BBOA	1.56	1.47	0.32
OOA-REG	1.85	1.54	0.52

600

601

602

603

604

605

606

607

608

609

610

611

PMF FACTOR	Oxalate (N=53) R^2	BC[a] (N=3928) R^2	Levoglucosan (N=38) R^2	Sulfate (N=3328)[b] R^2
HOA	0.01	0.58	0.12	0.004
BBOA	0.04	0.05	0.65	0.005
MO-OA	0.50	0.01	0.02	0.54
LO-OA	0.32	0.01	0.08	0.07
NOA	0.01	0.09	0.12	0.06
OOA-REG	0.62	0.02	0.01	0.65

[a.] BC data smoothed to remove underestimated BC concentrations during periods of high filter loading (Hyvärinen et al., 2013)

[b.] R^2 value calculated after initial high SO_4 period.

Figure Captions

Figure 1: The measurement site location is marked by a red square on the map, and the adjacent highway has been colored in red. A detailed view of the measurement site and the two measurement stations is shown in the lower right-hand corner in the upper right-hand corner is the wind rose and polar plots for black carbon and NO, with the red lines denoting the direction of the highway. Grenoble is to the north.

Figure 2: The non-refractory submicrometer aerosol concentration in μg m^{-3} of SO_4, NH_4, NO_3, and Organic species is plotted along with black carbon both for the campaign time series and the average concentration of each species for the whole campaign and during high traffic periods (A), 15 minute traffic concentration (missing data due to malfunction in the traffic cameras on those days) (B) COO^+ (*m/z* 44) and $C_4H_9^+$ (*m/z* 57) (C), and the number-weighted geometric size distribution (D) with the total number concentration of particles as a function of time (D, right axis).

Figure 3: The concentration in ppbv of PTR-ToF-MS VOC species identified isoprene and MVK/Methacrolin (left axis, A), VOC species associated with diesel exhaust ($CH_4NO_2^+$, $C_2H_5O^+$, B),VOC species associated with gasoline exhaust ($C_6H_7^+$, C_9H13^+, C). NO and NO_2 (gas-phase) ppbv concentrations (D) and ambient temperature (right axis, A) during the measurement period are also shown.

Figure 4: Diurnal profiles of boundary-layer scaled VOC peaks from PTR-ToF-MS measurements and BC peaks from MAAP measurements (A), temperature (right axis, B), boundary layer height (left axis, B), vehicular speed (left axis, C) and vehicle concentration (right axis, C).

Figure 5: The mass spectra of the six resolved factors, more oxidized organic aerosol (MO-OA), less oxidized organic aerosol (LO-OA), regional oxidized organic aerosol (reg-OOA), biomass burning organic aerosol (BBOA), hydrocarbon-like organic aerosol (HOA), and nitrogen-containing organic aerosol (NOA). Fraction of total signal is plotted against *m/z* and the peaks are color-coded to show their high-resolution identifications.

Figure 6: The diurnal profiles (A) and concentration and standard deviation of the six resolved aerosol factors (B).

Figure 7: The time series of the six-factor PMF solution (A), the resolved BBOA factor time series concentration (right axis, B) and off-line levoglucosan measurements (left axis, B), the resolved HOA factor time series concentration and BC (right axis, C), HR-TOF-AMS-measured SO_4 and the resolved regional OOA factor (left axis, D) and off-line oxalate measurements (right axis, right). The inset shows the calculated mass contribution during all (left) and high traffic (right) periods of each resolved PMF factor.

Figure 8:
Calculated HOA and measured BC concentrations from the campaign and HOA: BC ratios from previous field campaigns. Grey area is shaded to include a diesel-only environment and two French HOA: BC ratios: one from Crippa et al., (2013) and from this study (A). The HOA: BC ratio from various literature sources versus percent diesel fuel use out of total fuel use for the country of study (B).

Figure 9: Measured EC and OC, with calculated contribution of non-primary fossil organic carbon (assuming 100% fossil EC and HOA, A) and assuming partial modern organic carbon EC and HOA contribution (B). The possible fossil OOA (light blue) was calculated by the subtraction of HOA from the fossil-OC fraction (assuming HOA either all fossil, A, or 95% fossil, B, and EC either all fossil (a) or 5%+BBOA/3 modern (b).

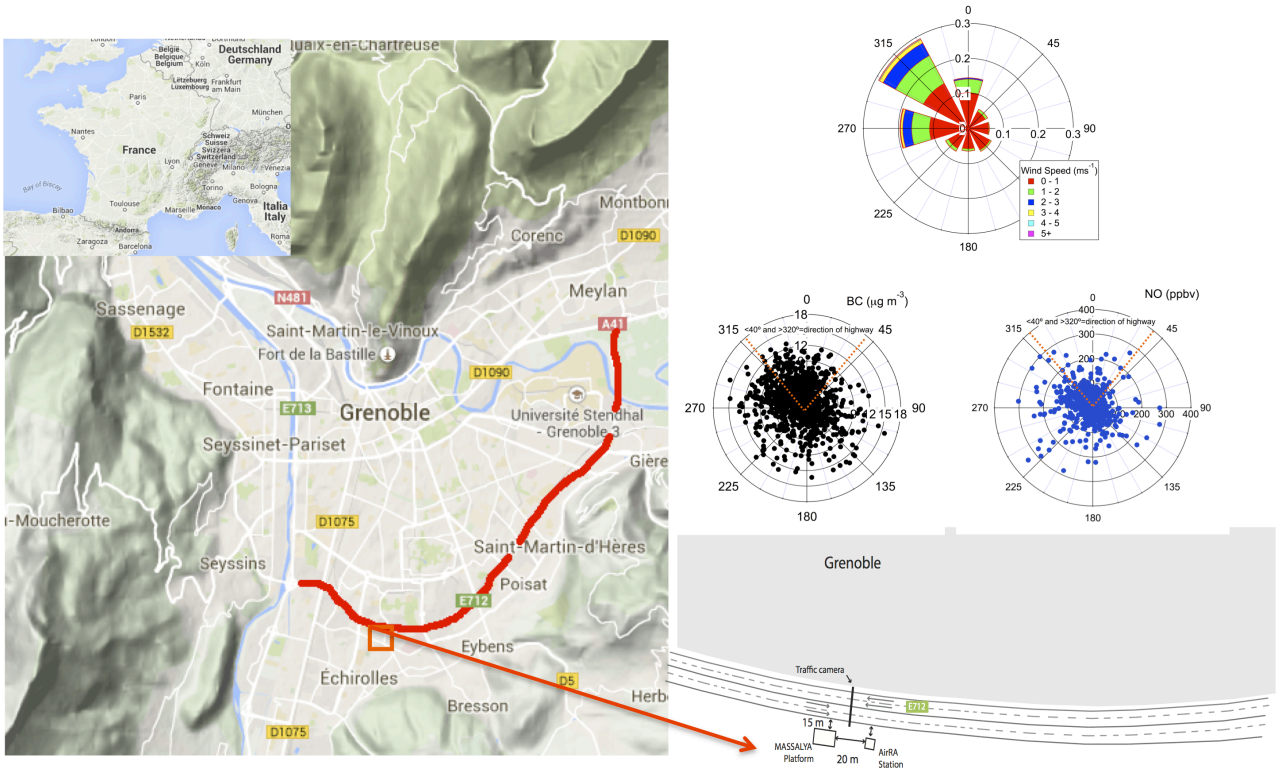

Figure 1
The measurement site location is marked by a red square on the map, and the adjacent highway has been colored in red. A detailed view of the measurement site and the two measurement stations is shown in the lower right-hand corner in the upper right-hand corner is the wind rose and polar plots for black carbon and NO, with the red lines denoting the direction of the highway. Grenoble is to the north.

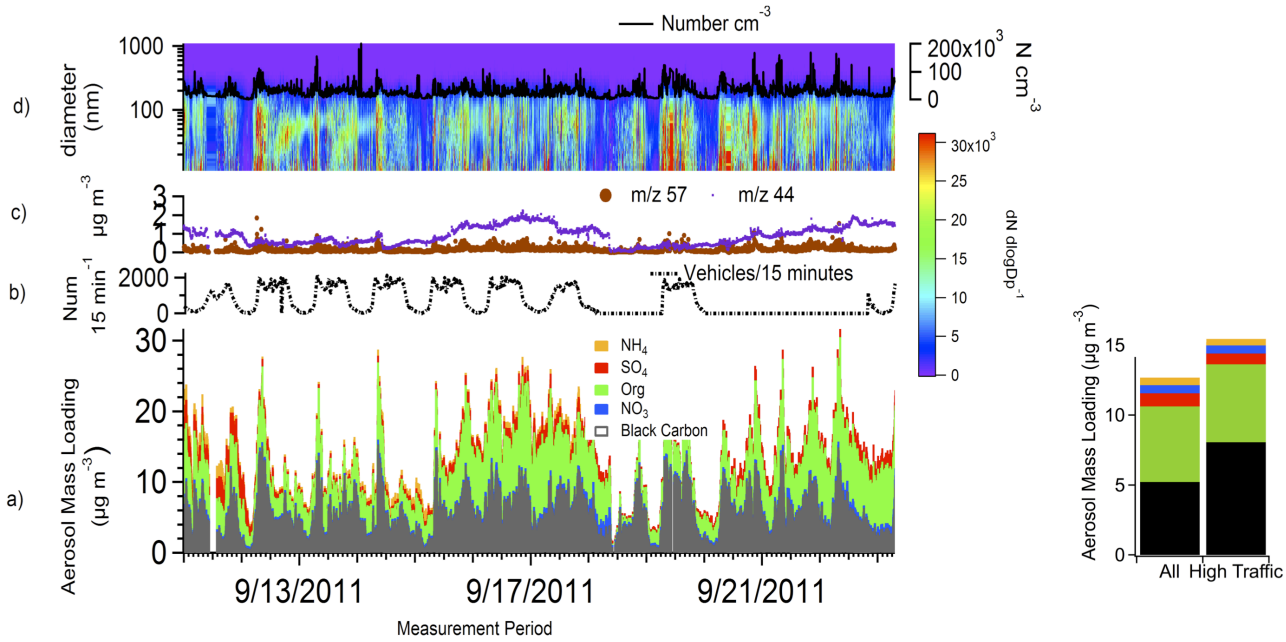

Figure 2: The non-refractory submicrometer aerosol concentration in μg m^{-3} of SO_4, NH_4, NO_3, and Organic species is plotted along with black carbon both for the campaign time series and the average concentration of each species for the whole campaign and during high traffic periods (A), 15 minute traffic concentration (missing data due to malfunction in the traffic cameras on those days) (B) COO^+ (*m/z* 44) and $C_4H_9^+$ (*m/z* 57) (C), and the number-weighted geometric size distribution (D) with the total number concentration of particles as a function of time (D, right axis).

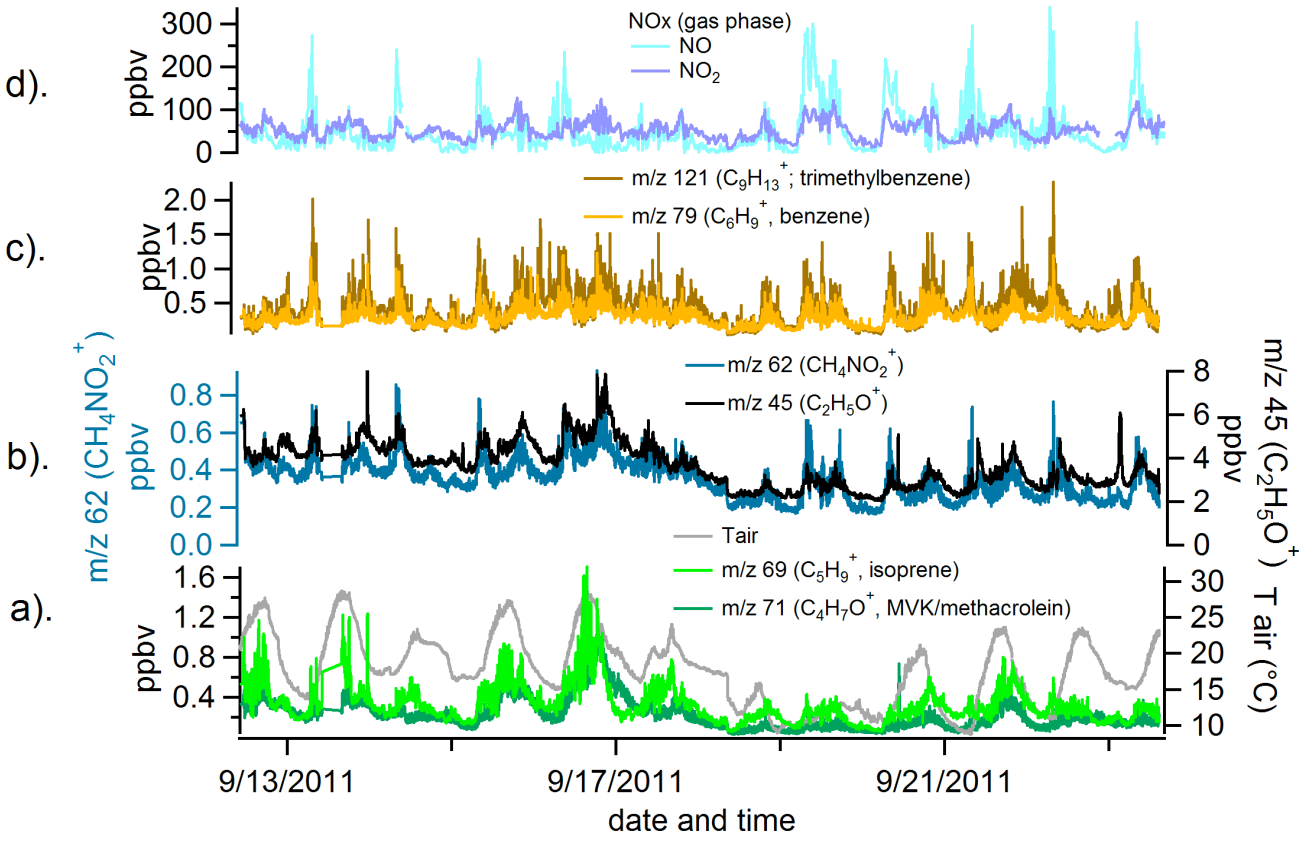

Figure 3
The concentration in ppbv of PTR-ToF-MS VOC species identified isoprene and MVK/Methacrolin (left axis, A), VOC species associated with diesel exhaust ($CH_4NO_2^+$, $C_2H_5O^+$, B),VOC species associated with gasoline exhaust ($C_6H_7^+$, C_9H13^+, C). NO and NO_2 (gas-phase) ppbv concentrations (D) and ambient temperature (right axis, A) during the measurement period are also shown.

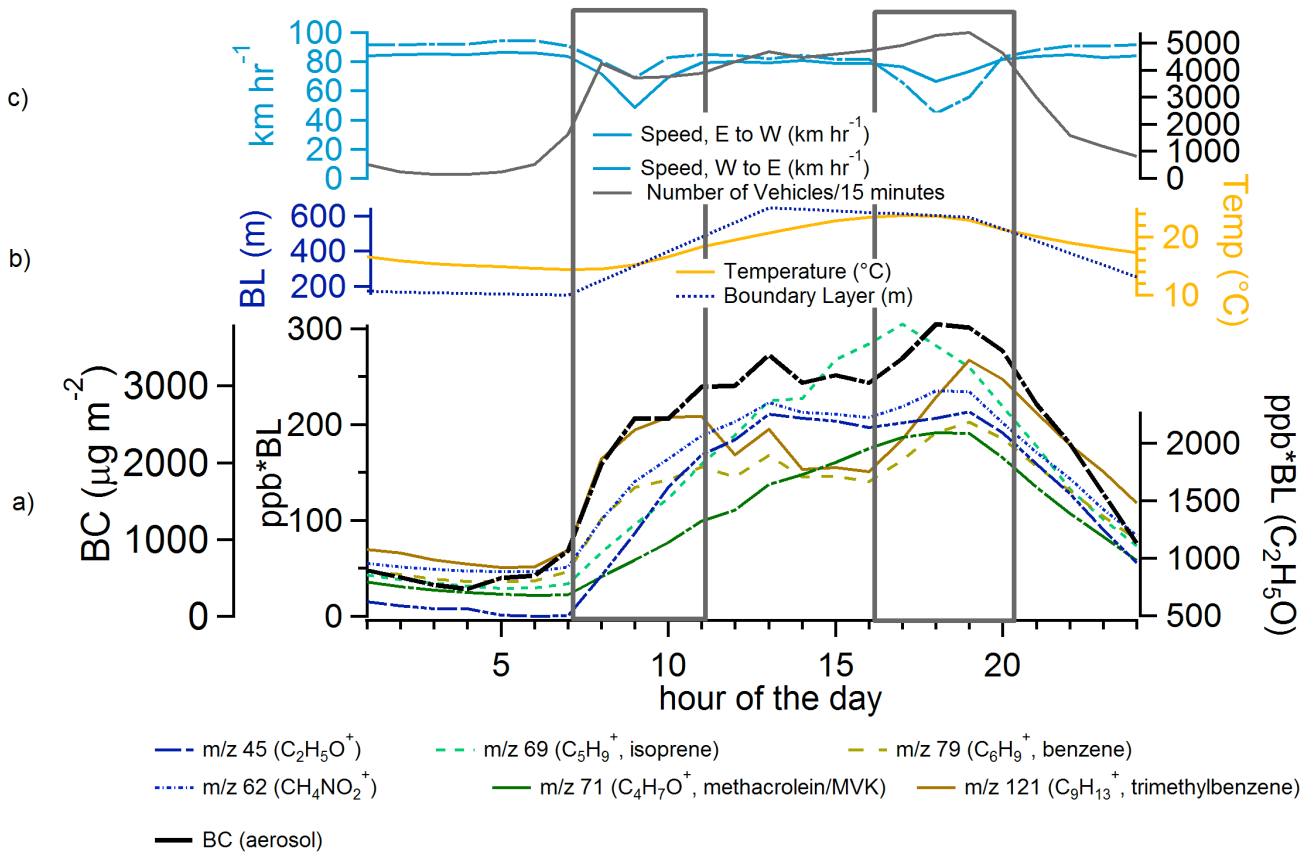

Figure 4 Diurnal profiles of boundary-layer scaled VOC peaks from PTR-MS measurements and BC peaks from MAAP measurements (A), temperature (right axis, B), boundary layer height (left axis, B), vehicular speed (left axis, C) and vehicle concentration (right axis, C).

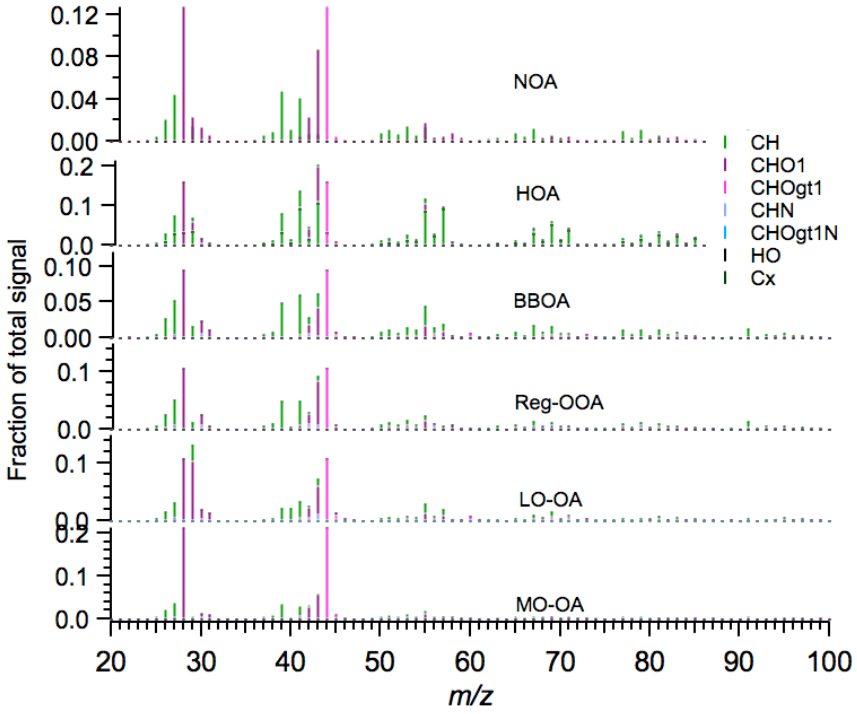

Figure 5:
The mass spectra of the six resolved factors, more oxidized organic aerosol (MO-OA), less oxidized organic aerosol (LO-OA), regional oxidized organic aerosol (reg-OOA), biomass burning organic aerosol (BBOA), hydrocarbon-like organic aerosol (HOA), and nitrogen-containing organic aerosol (NOA). Fraction of total signal is plotted against *m/z* and the peaks are color-coded to show their high-resolution identifications.

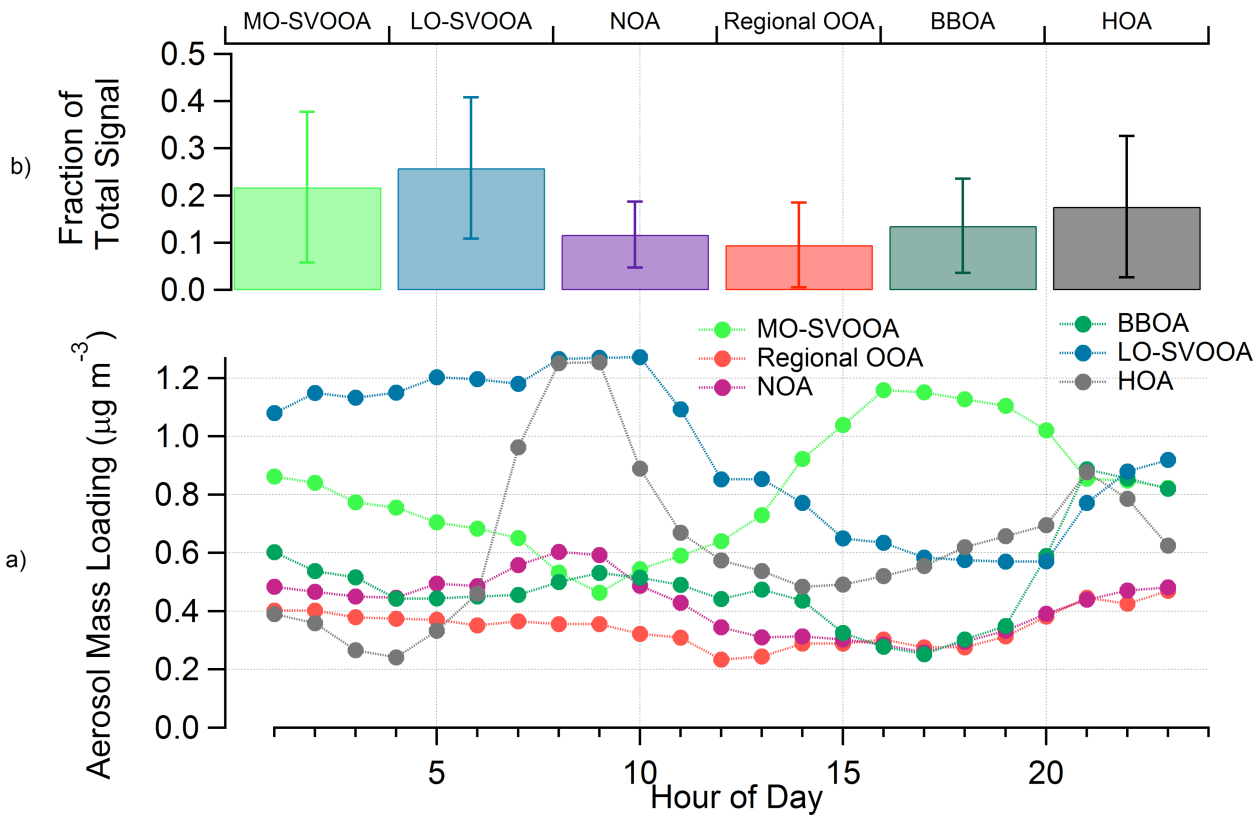

Figure 6: The diurnal profiles (A) and concentration and standard deviation of the six resolved aerosol factors (B).

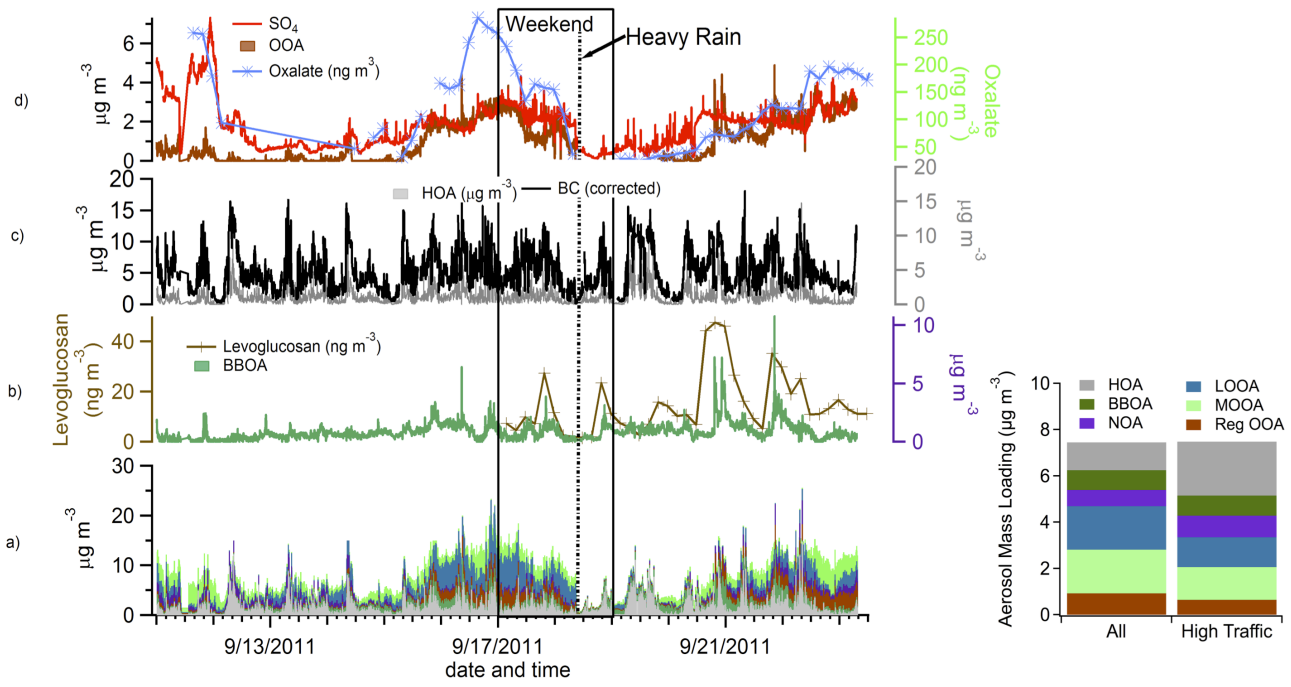

Figure 7:

The time series of the six-factor PMF solution (A), the resolved BBOA factor time series concentration (right axis, B) and off-line levoglucosan measurements (left axis, B), the resolved HOA factor time series concentration and BC (right axis, C), HR-TOF-AMS-measured SO_4 and the resolved regional OOA factor (left axis, D) and off-line oxalate measurements (right axis, right). The inset shows the calculated mass contribution during all (left) and high traffic (right) periods of each resolved PMF factor.

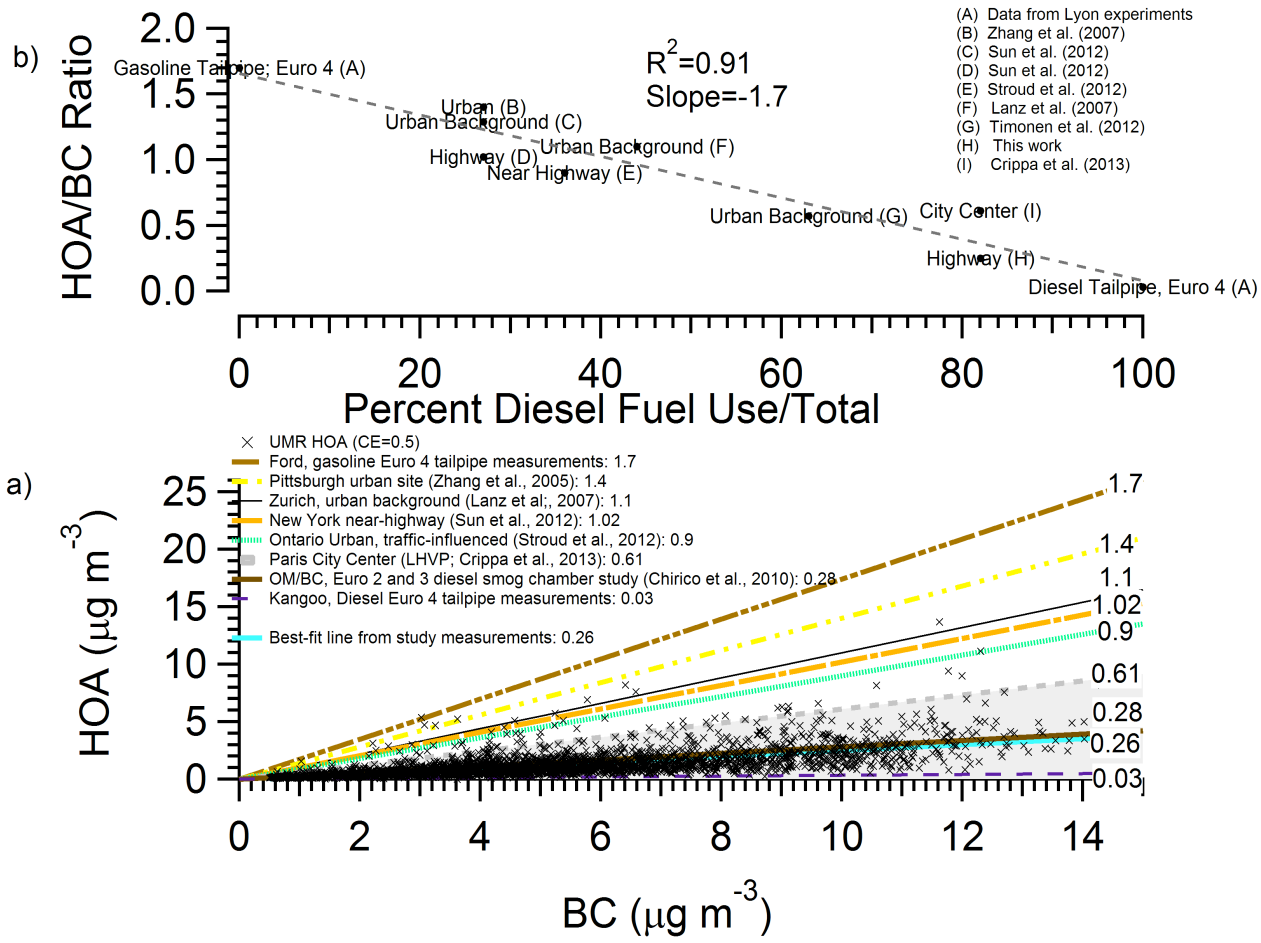

Figure 8
Calculated UMR HOA and measured BC concentrations from the campaign and HOA: BC ratios from previous field campaigns. Grey area is shaded to include a diesel-only environment and two French HOA: BC ratios: one from Crippa et al., (2013) and from this study (A). The HOA: BC ratio from various literature sources versus percent diesel fuel use out of total fuel use for the country of study (B).

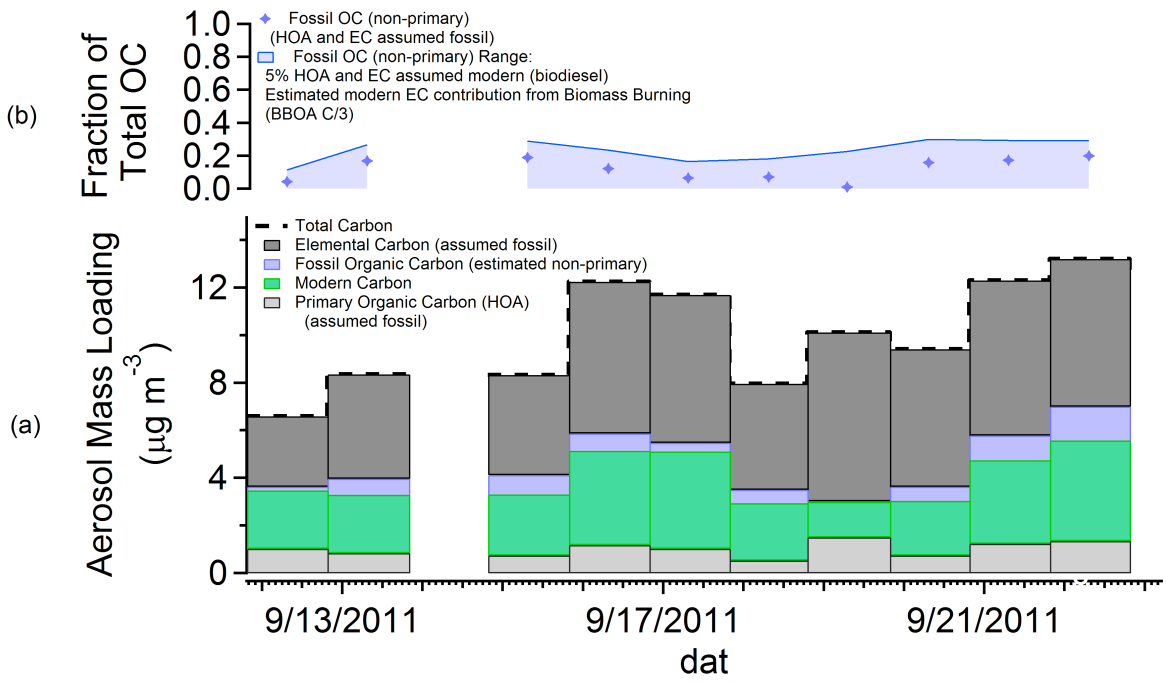

Figure 9: Measured EC and OC, with calculated contribution of non-primary fossil organic carbon (assuming 100% fossil EC and HOA, a) and assuming partial modern organic carbon EC and HOA contribution (b). The possible fossil OOA (light blue) was calculated by the subtraction of HOA from the fossil-OC fraction (assuming HOA either all fossil, A, or 95% fossil, B, and EC either all fossil (a) or 5%+BBOA/3 modern (b).

References

Aiken, A. C., Salcedo, D., Cubison, M. J., Huffman, J. a., DeCarlo, P. F., Ulbrich, I. M., Docherty, K. S., Sueper, D., Kimmel, J. R., Worsnop, D. R., Trimborn, a., Northway, M., Stone, E. a., Schauer, J. J., Volkamer, R., Fortner, E., de Foy, B., Wang, J., Laskin, a., Shutthanandan, V., Zheng, J., Zhang, R., Gaffney, J., Marley, N. a., Paredes-Miranda, G., Arnott, W. P., Molina, L. T., Sosa, G. and Jimenez, J. L.: Mexico City aerosol analysis during MILAGRO using high resolution aerosol mass spectrometry at the urban supersite (T0) – Part 1: Fine particle composition and organic source apportionment, Atmos. Chem. Phys., 9(2), 8377–8427, doi:10.5194/acpd-9-8377-2009, 2009.

Aiken, A. C., Decarlo, P. F., Kroll, J. H., Worsnop, D. R., Huffman, J. A., Docherty, K. S., Ulbrich, I. M., Mohr, C., Kimmel, J. R., Sueper, D., Sun, Y., Zhang, Q., Trimborn, A., Northway, M., Ziemann, P. J., Canagaratna, M. R., Onasch, T. B., Alfarra, M. R., Prevot, A. S. H., Dommen, J., Duplissy, J., Metzger, A., Baltensperger, U. and Jimenez, J. L.: O/C and OM/OC ratios of primary, secondary, and ambient organic aerosols with high-resolution time-of-flight aerosol mass spectrometry., Environ. Sci. Technol., 42(12), 4478–85.

Bahreini, R., Middlebrook, a. M., de Gouw, J. a., Warneke, C., Trainer, M., Brock, C. a., Stark, H., Brown, S. S., Dube, W. P., Gilman, J. B., Hall, K., Holloway, J. S., Kuster, W. C., Perring, a. E., Prevot, a. S. H., Schwarz, J. P., Spackman, J. R., Szidat, S., Wagner, N. L., Weber, R. J., Zotter, P. and Parrish, D. D.: Gasoline emissions dominate over diesel in formation of secondary organic aerosol mass, Geophys. Res. Lett., 39(6), doi:10.1029/2011GL050718, 2012.

Birch, M. E. and Cary, R. A.: Elemental Carbon-Based Method for Monitoring Occupational Exposures to Particulate Diesel Exhaust, Aerosol Sci. Technol., 25(3), 221–241, 1996.

Bond, T. C., Doherty, S. J., Fahey, D. W., Forster, P. M., Berntsen, T., DeAngelo, B. J., Flanner, M. G., Ghan, S., Kärcher, B., Koch, D., Kinne, S., Kondo, Y., Quinn, P. K., Sarofim, M. C., Schultz, M. G., Schulz, M., Venkataraman, C., Zhang, H., Zhang, S., Bellouin, N., Guttikunda, S. K., Hopke, P. K., Jacobson, M. Z., Kaiser, J. W., Klimont, Z., Lohmann, U., Schwarz, J. P., Shindell, D., Storelvmo, T., Warren, S. G. and Zender, C. S.: Bounding the role of black carbon in the climate system: A scientific assessment, J. Geophys. Res. Atmos., 118(11), 5380–5552, doi:10.1002/jgrd.50171, 2013.

Broderick, B. and Marnane, I.: A comparison of the C2–C9 hydrocarbon compositions of vehicle fuels and urban air in Dublin, Ireland, Atmos. Environ., 36(6), 975–986, doi:10.1016/S1352-2310(01)00472-1, 2002.

Brugge, D., Durant, J. L. and Rioux, C.: Near-highway pollutants in motor vehicle exhaust: a review of epidemiologic evidence of cardiac and pulmonary health risks., Environ. Health, 6, 23, doi:10.1186/1476-069X-6-23, 2007.

Bruns, E. A, Perraud, V., Zelenyuk, A., Ezell, M. J., Johnson, S. N., Yu, Y., Imre, D., Finlayson-Pitts, B. J. and Alexander, M. L.: Comparison of FTIR and particle mass spectrometry for the measurement of particulate organic nitrates., Environ. Sci. Technol., 44(3), 1056–61, doi:10.1021/es9029864, 2010.

Carlton, A. G., Wiedinmyer, C. and Kroll, J. H.: A review of Secondary Organic Aerosol (SOA) formation from isoprene, Atmos. Chem. Phys. Discuss., 9(2), 8261–8305, doi:10.5194/acpd-9-8261-2009, 2009.

921 Cavalli, F., Viana, M., Yttri, K. E., Genberg, J. and Putaud, J.-P.: Toward a standardised thermal-optical
922 protocol for measuring atmospheric organic and elemental carbon: the EUSAAR protocol, Atmos. Meas. Tech.,
923 3(1), 79–89, 2010.

924 Chameides, W., Lindsay, R., Richardson, J. and Kiang, C.: The role of biogenic hydrocarbons in urban
925 photochemical smog: Atlanta as a case study, Science (80-83)., 241(4872), 1473–1475,
926 doi:10.1126/science.3420404, 1988.

927 Chen, J., Zhao, C. S., Ma, N. and Yan, P.: Aerosol hygroscopicity parameter derived from the light scattering
928 enhancement factor measurements in the North China Plain, Atmos. Chem. Phys., 14(15), 8105–8118,
929 doi:10.5194/acp-14-8105-2014, 2014.

930 Cheung, K.L., Ntziachristos, L.,Tzamkiozis, T., Schauer, J.J., Samaras, Z., Moore, K.F. & Sioutas, C. (2010)
931 Emissions of Particulate Trace Elements, Metals and Organic Species from Gasoline, Diesel, and Biodiesel Pas-
932 senger Vehicles and Their Relation to Oxidative Potential, Aerosol Science and Technology, 44:7, 500-513,
933 DOI: 10.1080/02786821003758294

934 Chirico, R., Decarlo, P. F., Heringa, M. F., Tritscher, T., Richter, R. and Pr, A. S. H.: Impact of aftertreatment
935 devices on primary emissions and secondary organic aerosol formation potential from in-use diesel vehicles :
936 results from smog chamber experiments, Atmos. Chem. Phys., 11545–11563, doi:10.5194/acp-10-11545-2010,
937 2010.

938 Crippa, M., DeCarlo, P. F., Slowik, J. G., Mohr, C., Heringa, M. F., Chirico, R., Poulain, L., Freutel, F., Sciare,
939 J., Cozic, J., Di Marco, C. F., Elsasser, M., Nicolas, J. B., Marchand, N., Abidi, E., Wiedensohler, A., Drewnick,
940 F., Schneider, J., Borrmann, S., Nemitz, E., Zimmermann, R., Jaffrezo, J.-L., Prévôt, A. S. H. and Baltensperger,
941 U.: Wintertime aerosol chemical composition and source apportionment of the organic fraction in the
942 metropolitan area of Paris, Atmos. Chem. Phys., 13(2), 961–981, doi:10.5194/acp-13-961-2013, 2013.

943 Decarlo, P. F., Kimmel, J. R., Trimborn, A., Northway, M. J., Jayne, J. T., Aiken, A. C., Gonin, M., Fuhrer, K.,
944 Horvath, T., Docherty, K. S., Worsnop, D. R. and Jimenez, J. L.: Field-Deployable, high-resolution, time-of-
945 flight aerosol mass spectrometer, Anal. Chem., 78(24), 8281–8289, doi:8410.1029/2001JD001213. 2006.

946 Docherty, K. S., Stone, E. A., Ulbrich, I. M., DeCarlo, P. F., Snyder, D. C., Schauer, J. J., Peltier, R. E., Weber,
947 R. J., Murphy, S. M., Seinfeld, J. H., Grover, B. D., Eatough, D. J. and Jimenez, J. L.: Apportionment of Primary
948 and Secondary Organic Aerosols in Southern California during the 2005 Study of Organic Aerosols in Riverside
949 (SOAR-1), Environ. Sci. Technol., 42(20), 7655–7662, doi:10.1021/es8008166, 2008.

950 El Haddad, I., Marchand, N., Dron, J., Temime-Roussel, B., Quivet, E., Wortham, H., Jaffrezo, J. L., Baduel, C.,
951 Voisin, D., Besombes, J. L. and Gille, G.: Comprehensive primary particulate organic characterization of
952 vehicular exhaust emissions in France, Atmos. Environ., 43(39), 6190–6198,
953 doi:10.1016/j.atmosenv.2009.09.001, 2009.

954 El Haddad, I., Marchand, N., Wortham, H., Piot, C., Besombes, J.-L., Cozic, J., Chauvel, C., Armengaud, a.,
955 Robin, D. and Jaffrezo, J.-L.: Primary sources of $PM_{2.5}$ organic aerosol in an industrial Mediterranean city,
956 Marseille, Atmos. Chem. Phys., 11(5), 2039–2058, doi:10.5194/acp-11-2039-2011, 2011.

957 El Haddad, I., D'Anna, B., Temime-Roussel, B., Nicolas, M., Boreave, A., Favez, O., Voisin, D., Sciare, J.,
958 George, C., Jaffrezo, J.-L., Wortham, H., and Marchand, N.: Towards a better understanding of the origins,
959 chemical composition and aging of oxygenated organic aerosols: case study of a Mediterranean industrialized
960 environment, Marseille, Atmos. Chem. Phys., 13, 7875-7894, doi:10.5194/acp-13-7875-2013, 2013.

961 Farmer, D. K., Matsunaga, a, Docherty, K. S., Surratt, J. D., Seinfeld, J. H., Ziemann, P. J. and Jimenez, J. L.:
962 Response of an aerosol mass spectrometer to organonitrates and organosulfates and implications for atmospheric
963 chemistry., Proc. Natl. Acad. Sci. U. S. A., 107(15), 6670–5, doi:10.1073/pnas.0912340107, 2010.

964 Favez, O., El Haddad, I., Piot, C., Boréave, a., Abidi, E., Marchand, N., Jaffrezo, J.-L., Besombes, J.-L.,
965 Personnaz, M.-B., Sciare, J., Wortham, H., George, C. and D'Anna, B.: Inter-comparison of source
966 apportionment models for the estimation of wood burning aerosols during wintertime in an Alpine city
967 (Grenoble, France), Atmos. Chem. Phys., 10(12), 5295–5314, doi:10.5194/acp-10-5295-2010, 2010.

968 Fry, J. L., Draper, D. C., Zarzana, K. J., Campuzano-Jost, P., Day, D. a., Jimenez, J. L., Brown, S. S., Cohen, R.
969 C., Kaser, L., Hansel, A., Cappellin, L., Karl, T., Hodzic Roux, A., Turnipseed, A., Cantrell, C., Lefer, B. L. and
970 Grossberg, N.: Observations of gas- and aerosol-phase organic nitrates at BEACHON-RoMBAS 2011, Atmos.
971 Chem. Phys., 13(17), 8585–8605, doi:10.5194/acp-13-8585-2013, 2013.

972 Gentner, D. R., Isaacman, G., Worton, D. R., Chan, A. W. H., Dallmann, T. R., Davis, L., Liu, S., Day, D. a,
973 Russell, L. M., Wilson, K. R., Weber, R., Guha, A., Harley, R. a and Goldstein, A. H.: Elucidating secondary
974 organic aerosol from diesel and gasoline vehicles through detailed characterization of organic carbon emissions.,
975 Proc. Natl. Acad. Sci. U. S. A., 109(45), 18318–23, doi:10.1073/pnas.1212272109, 2012.

976 Goldstein, A. H., Koven, C. D., Heald, C. L. and Fung, I. Y.: Biogenic carbon and anthropogenic pollutants
977 combine to form a cooling haze over the southeastern United States, Proc. Natl. Acad. Sci., 106(22), 8835–8840,
978 doi:10.1073/pnas.0904128106, 2009.

979 Hellebust, S., Temime-Roussel, B., Bertrand, A., Platt, S. M., El Haddad, I., Pieber, S., Zardini, A. A., Suarez-
980 Bertoa, R., Slowik, J. G., Huang, R. J., Astorga, C., Prevot, A. S. H. and Marchand, N.: Comparison of Gasoline
981 and Diesel Vehicles-Emission Factors of Volatile Organic Compounds from EURO5 Diesel and Gasoline
982 Vehicles and Their Potential Integrated Influence on Air Quality, Am. Assoc. Aerosol Res., Fall 2013 , 2013.

983 Hellebust, S., Temime-Roussel, B., Bertrand, A., Platt, S. M., El Haddad, I., Pieber, S., Zardini, A. A., Suarez-
984 Bertoa, R., Slowik, J. G., Huang, R. J., Astorga, C., Prevot, A. S. H. and Marchand, N.: Emission factors of Vol-
985 atile Organic Compounds measured by Proton Transfer Reaction – Time -of-Flight – Mass Spectrometry 1. Euro
986 2 scooter, Euro 5 light duty gasoline and diesel vehicles and Euro V heavy duty diesel vehicles (in preparation).

987 Hennigan, C. J., Sullivan, A. P., Collett, J. L. and Robinson, A. L.: Levoglucosan stability in biomass burning
988 particles exposed to hydroxyl radicals, Geophys. Res. Lett., 37(9), doi:10.1029/2010GL043088, 2010.

989 Herich, H., Gianini, M. F. D., Piot, C., Močnik, G., Jaffrezo, J.-L., Besombes, J.-L., Prévôt, A. S. H. and
990 Hueglin, C.: Overview of the impact of wood burning emissions on carbonaceous aerosols and PM in large parts
991 of the Alpine region, Atmos. Environ., 89, 64–75, doi:10.1016/j.atmosenv.2014.02.008, 2014.

992 Hodzic, A., Jimenez, J. L., Madronich, S., Canagaratna, M. R., DeCarlo, P. F., Kleinman, L. and Fast, J.:
993 Modeling organic aerosols in a megacity: potential contribution of semi-volatile and intermediate volatility
994 primary organic compounds to secondary organic aerosol formation, Atmos. Chem. Phys., 10(12), 5491–5514,
995 doi:10.5194/acp-10-5491-2010, 2010.

996 Huffman, J. A., Jayne, J. T., Drewnick, F., Aiken, A. C., Onasch, T., Worsnop, D. R. and Jimenez, J. L.: Design,
997 Modeling, Optimization, and Experimental Tests of a Particle Beam Width Probe for the Aerodyne Aerosol
998 Mass Spectrometer, Aerosol Sci. Technol., 39(12), 1143–1163, doi:10.1080/02786820500423782, 2005.

999 Hyvärinen, A.-P., Vakkari, V., L. Laakso, R. K. Hooda, Sharma, V. P., Panwar, T. S., Beukes, J. P., van Zyl, P.
1000 G., Josipovic, M., Garland, R. M., Andreae, M. O., Pöschl, U. and Petzold, A.: Correction for a measurement

1001 artifact of the Multi-Angle Absorption Photometer (MAAP) at high black carbon mass concentration levels,
1002 Atmos. Meas. Tech., 6(1), 81–90, doi:10.5194/amt-6-81-2013, 2013.

1003 Inomata, S., Tanimoto, H., Fujitani, Y., Sekimoto, K., Sato, K., Fushimi, A., Yamada, H., Hori, S., Kumazawa,
1004 Y., Shimono, A. and Hikida, T.: On-line measurements of gaseous nitro-organic compounds in diesel vehicle
1005 exhaust by proton-transfer-reaction mass spectrometry, Atmos. Environ., 73(x), 195–203,
1006 doi:10.1016/j.atmosenv.2013.03.035, 2013.

1007 Jaffrezo, J. L., Davidson, C. I., Kuhns, H. D., Bergin, M. H., Hillamo, R., Maenhaut, W., Kahl, J. W. and Harris,
1008 J. M.: Biomass burning signatures in the atmosphere of central Greenland. J. Geophys. Res: Atmos., 103, 1998.

1009 Jaffrezo, J.-L., Aymoz, G. and Cozic, J.: Size distribution of EC and OC in the aerosol of Alpine valleys during
1010 summer and winter, Atmos. Chem. Phys., 5(11), 2915–2925, 2005

1011 Janssen, N. A. H., World Health Organization, Regional Office for Europe and Joint WHO/Convention Task
1012 Force on the Health Aspects of Air Pollution: Health effects of black carbon. [online] Available from:
1013 http://www.euro.who.int/__data/assets/pdf_file/0004/162535/e96541.pdf, 2012.

1014 Karner, A. A., Eisinger, D. S., and Niemeier, D. A. (2010). "Near-RoadwayAir Quality: Synthesizing the
1015 Findings from Real-World Data." Environ. Sci. and Tech, 44, 5334–5344.
1016
1017 Kroll, J. H., Ng, N. L., Murphy, S. M., Flagan, R. C. and Seinfeld, J. H.: Secondary organic aerosol formation
1018 from isoprene photooxidation under high-NO x conditions, Geophys. Res. Lett., 32(18),
1019 doi:10.1029/2005GL023637, 2005.

1020 Lanz, V. A., Alfarra, M. R., Baltensperger, U., Buchmann, B., Hueglin, C. and Prevot, A. S. H.: Source
1021 apportionment of submicron organic aerosols at an urban site by factor analytical modelling of aerosol mass
1022 spectra, Atmos. Chem. Phys., 1503–1522, 2007.

1023 Lighty, J. S., Veranth, J. M. and Sarofim, A. F.: Combustion Aerosols: Factors Governing Their Size and
1024 Composition and Implications to Human Health, J. Air Waste Manage. Assoc., 50(9), 1565–1618,
1025 doi:10.1080/10473289.2000.10464197, 2000.

1026 Liu, L., Lacis, A.A., Carlson, B. E., Mishchenko, M. I. and Cairns, B.: Assessing Goddard Institute for Space
1027 Studies ModelE aerosol climatology using satellite and ground-based measurements: A comparison study, J.
1028 Geophys. Res., 111(D20), D20212, doi:10.1029/2006JD007334, 2006.

1029 Matthew, B. M., Middlebrook, A. M. and Onasch, T. B.: Collection Efficiencies in an Aerodyne Aerosol Mass
1030 Spectrometer as a Function of Particle Phase for Laboratory Generated Aerosols, Aerosol Sci. Technol., 42(11),
1031 884–898, doi:10.1080/02786820802356797, 2008.

1032 Minguillón, M. C., Perron, N., Querol, X., Szidat, S., Fahrni, S. M., Alastuey, A., Jimenez, J. L., Mohr, C.,
1033 Ortega, A. M., Day, D. A., Lanz, V. A., Wacker, L., Reche, C., Cusack, M., Amato, F., Kiss, G., Hoffer, A.,
1034 Decesari, S., Moretti, F., Hillamo, R., Teinilä, K., Seco, R., Peñuelas, J., Metzger, A., Schallhart, S., Müller, M.,
1035 Hansel, A., Burkhart, J. F., Baltensperger, U., and Prévôt, A. S. H.: Fossil versus contemporary sources of fine
1036 elemental and organic carbonaceous particulate matter during the DAURE campaign in Northeast Spain, Atmos.
1037 Chem. Phys., 11, 12067-12084, doi:10.5194/acp-11-12067-2011, 2011.

1038 Mohr, C., Huffman, J. A., Cubison, M. J., Aiken, A. C., Kenneth, S., Kimmel, J. R., Ulbrich, I. M., Hannigan,
1039 M. and Jimenez, J. L.: Characterization of Primary Organic Aerosol Emissions from Meat Cooking , Trash
1040 Burning , and Motor Vehicles with High-Resolution Aerosol Mass Spectrometry and Comparison with Ambient
1041 and Chamber Observations Characterization of Primary Organic Aerosol, Environ. Sci. and Tech., 2009.

1042 Ng, N. L., Kroll, J. H., Chan, A. W. H., Chhabra, P. S., Flagan, R. C. and Seinfeld, J. H.: and Physics Secondary
1043 organic aerosol formation from m -xylene , toluene , and benzene, , (3), 3909–3922, 2007.

1044 Ng, N. L., Kwan, A. J., Surratt, J. D., Chan, A. W. H., Chhabra, P. S., Sorooshian, A., Pye, H. O. T., Crounse, J.
1045 D., Wennberg, P. O., Flagan, R. C. and Seinfeld, J. H.: Secondary organic aerosol (SOA) formation from
1046 reaction of isoprene with nitrate radicals (NO_3), Atmos. Chem. Phys., 8(14), 4117–4140, doi:10.5194/acp-8-
1047 4117-2008, 2008.

1048 Nordin, E. Z., Eriksson, a. C., Roldin, P., Nilsson, P. T., Carlsson, J. E., Kajos, M. K., Hellén, H., Wittbom, C.,
1049 Rissler, J., Löndahl, J., Swietlicki, E., Svenningsson, B., Bohgard, M., Kulmala, M., Hallquist, M. and Pagels, J.
1050 H.: Secondary organic aerosol formation from idling gasoline passenger vehicle emissions investigated in a
1051 smog chamber, Atmos. Chem. Phys., 13(12), 6101–6116, doi:10.5194/acp-13-6101-2013, 2013.

1052 Parrish, D. D., Stohl, A., Forster, C., Atlas, E. L., Blake, D. R., Goldan, P. D., Kuster, W. C. and de Gouw, J. A.:
1053 Effects of mixing on evolution of hydrocarbon ratios in the troposphere, J. Geophys. Res. Atmos., 112(D10),
1054 doi:10.1029/2006JD007583, 2007.

1055 Platt, S. M., El Haddad, I., Zardini, A.A., Clairotte, M., Astorga, C., Wolf, R., Slowik, J. G., Temime-Roussel,
1056 B., Marchand, N., Ježek, I., Drinovec, L., Močnik, G., Möhler, O., Richter, R., Barmet, P., Bianchi, F.,
1057 Baltensperger, U. and Prévôt, a. S. H.: Secondary organic aerosol formation from gasoline vehicle emissions in a
1058 new mobile environmental reaction chamber, Atmos. Chem. Phys., 13(18), 9141–9158, doi:10.5194/acp-13-
1059 9141-2013, 2013.

1060 Polo-Rehn, L.: Caractérisation des polluants dus au transport routier : Apports méthodologiques et cas d'études
1061 en Rhône Alpes, PhD thesis, Grenoble Univ., 2013.

1062 Presto, A. A., Miracolo, M. A., Donahue, N. M. and Robinson, A. L.: Secondary Organic Aerosol Formation
1063 from High-NOx Photo-Oxidation of Low Volatility Precursors: n-Alkanes, Environ. Sci. Technol., 44(6), 2029–
1064 2034, doi:10.1021/es903712r, 2010.

1065 Russell, L. M., Bahadur, R. and Ziemann, P. J.: Identifying organic aerosol sources by comparing functional
1066 group composition in chamber and atmospheric particles., Proc. Natl. Acad. Sci. U. S. A., 108(9), 3516–21,
1067 doi:10.1073/pnas.1006461108, 2011.

1068 Saarikoski, S., Carbone, S., Decesari, S., Giulianelli, L., Angelini, F., Canagaratna, M., Ng, N. L., Trimborn, a.,
1069 Facchini, M. C., Fuzzi, S., Hillamo, R. and Worsnop, D.: Chemical characterization of springtime
1070 submicrometer aerosol in Po Valley, Italy, Atmos. Chem. Phys., 12(18), 8401–8421, doi:10.5194/acp-12-8401-
1071 2012, 2012.

1072 Shilling, J. E., Zaveri, R.A., Fast, J. D., Kleinman, L., Alexander, M. L., Canagaratna, M. R., Fortner, E., Hubbe,
1073 J. M., Jayne, J. T., Sedlacek, a., Setyan, a., Springston, S., Worsnop, D. R. and Zhang, Q.: Enhanced SOA
1074 formation from mixed anthropogenic and biogenic emissions during the CARES campaign, Atmos. Chem.
1075 Phys., 13(4), 2091–2113, doi:10.5194/acp-13-2091-2013, 2013.

1076 Stroud, C. A., Moran, M. D., Makar, P. A., Gong, S., Gong, W., Zhang, J., Slowik, J. G., Abbatt, J. P. D., Lu, G.,
1077 Brook, J. R., Mihele, C., Li, Q., Sills, D., Strawbridge, K. B., McGuire, M. L. and Evans, G. J.: Evaluation of
1078 chemical transport model predictions of primary organic aerosol for air masses classified by particle component-
1079 based factor analysis, Atmos. Chem. Phys., 12(18), 8297–8321, doi:10.5194/acp-12-8297-2012, 2012.

1080 Sun, Y. L., Zhang, Q., Schwab, J. J., Chen, W.-N., Bae, M.-S., Hung, H.-M., Lin, Y.-C., Ng, N. L., Jayne, J.,
1081 Massoli, P., Williams, L. R. and Demerjian, K. L.: Characterization of near-highway submicron aerosols in New

1082 York City with a high-resolution aerosol mass spectrometer, Atmos. Chem. Phys., 12(4), 2215–2227,
1083 doi:10.5194/acp-12-2215-2012, 2012.

1084 Sun, Y., Zhang, Q., Zheng, M., Ding, X., Edgerton, E. S. and Wang, X.: Characterization and source
1085 apportionment of water-soluble organic matter in atmospheric fine particles (PM2.5) with high-resolution
1086 aerosol mass spectrometry and GC-MS., Environ. Sci. Technol., 45(11), 4854–61, doi:10.1021/es200162h,
1087 2011.

1088 Thornhill, D. A., Williams, A. E., Onasch, T. B., Wood, E., Herndon, S. C., Kolb, C. E., Knighton, W. B.,
1089 Zavala, M., Molina, L. T. and Marr, L. C.: Application of positive matrix factorization to on-road measurements
1090 for source apportionment of diesel- and gasoline-powered vehicle emissions in Mexico City, Atmos. Chem.
1091 Phys., 10(8), 3629–3644, doi:10.5194/acp-10-3629-2010, 2010.

1092 Ulbrich, I. M., Canagaratna, M. R., Zhang, Q., Worsnop, D. R. and Jimenez, J. L.: Interpretation of organic
1093 components from Positive Matrix Factorization of aerosol mass spectrometric data, Atmos. Chem. Phys., 9(9),
1094 2891–2918, doi:10.5194/acp-9-2891-2009, 2009.

1095 Vestreng, V., Ntziachristos, L., Semb, A., Reis, S., Isaksen, I. S. A. and Tarras, L.: Evolution of NOx emissions
1096 in Europe with focus on road transport control measures, Atmos. Chem. Phys., 1503–1520, 2009.

1097 WHO: Health Effects of Particulate Matter: Policy imlications for countries in eastern Europe, Caucasus and
1098 central Asia, World Health. Organ., 15 [online] Available from: www.euro.who.int, 2013.

1099 World Bank: World Development Report 2011: World Development Indicators, Fossil Fuel Energy
1100 Consumption., 2011.

1101 Xu, J., Zhang, Q., Chen, M., Ge, X., Ren, J. and Qin, D.: Chemical composition, sources, and processes of urban
1102 aerosols during summertime in Northwest China: insights from High Resolution Aerosol Mass Spectrometry,
1103 Atmos. Chem. Phys. Discuss., 14(11), 16187–16242, doi:10.5194/acpd-14-16187-2014, 2014.

1104 Zhang, Q., Worsnop, D. R., Canagaratna, M. R. and Jimenez, J.-L.: Hydrocarbon-like and oxygenated organic
1105 aerosols in Pittsburgh: insights into sources and processes of organic aerosols, Atmos. Chem. Phys. Discuss.,
1106 5(5), 8421–8471, doi:10.5194/acpd-5-8421-2005, 2005.

1107
1108
1109